Cerebral Cortex January 2014;24:17–36
doi:10.1093/cercor/bhs270
Advance Access publication September 25, 2012

A Weighted and Directed Interareal Connectivity Matrix for Macaque Cerebral Cortex

N. T. Markov[1,2,3], M. M. Ercsey-Ravasz[4,7], A. R. Ribeiro Gomes[1,2], C. Lamy[1,2], L. Magrou[1,2], J. Vezoli[1,2,8], P. Misery[1,2], A. Falchier[1,2,9], R. Quilodran[1,2,10], M. A. Gariel[1,2,11], J. Sallet[1,2,12], R. Gamanut[1,2], C. Huissoud[1,2,13], S. Clavagnier[1,2,14], P. Giroud[1,2], D. Sappey-Marinier[5], P. Barone[1,2,15], C. Dehay[1,2], Z. Toroczkai[4], K. Knoblauch[1,2], D. C. Van Essen[6] and H. Kennedy[1,2]

[1]Stem cell and Brain Research Institute, INSERM U846, 69500 Bron, France [2]Université de Lyon, Université Lyon I, 69003, Lyon, France [3]Department of Neurobiology, University of Yale, New Haven, CT 06520, USA [4]Department of Physics, Interdisciplinary Center for Network Science and Applications, University of Notre Dame, Notre Dame, IN 46556, USA [5]CERMEP, Hôpital Neurologique, 69394 Lyon Cedex 03, France [6]Washington University School of Medicine, St Louis, MO, USA [7]Current address: Physics Department, Babes-Bolyai University, Cluj-Napoca, Romania [8]Current address: Ernst Strüngmann Institute (ESI) for Neuroscience in Cooperation with the Max Planck Society, Frankfurt, Germany [9]Current address: Nathan S. Kline Institute for Psychiatric Research, Orangeburg, NY, USA [10]Current address: Escuela de Medicina, Departamento de Pre-clínicas, Universidad de Valparaíso, Valparaíso, Chile [11]Current address: Department of Vision and Cognition, Netherlands Institute for Neuroscience, Amsterdam, The Netherlands [12]Current address: Decision and Action Laboratory, University of Oxford, Oxford, UK [13]Current address: Service de gynécologie-obstétrique, hospices civils de Lyon, France [14]Current address: McGill Vision Research, Montreal, Canada [15]Current address: Cerveau et Cognition, UMR 5549, Toulouse, France

Address correspondence to Henry Kennedy. Email: henry.kennedy@inserm.fr

Retrograde tracer injections in 29 of the 91 areas of the macaque cerebral cortex revealed 1,615 interareal pathways, a third of which have not previously been reported. A weight index (extrinsic fraction of labeled neurons [FLNe]) was determined for each area-to-area pathway. Newly found projections were weaker on average compared with the known projections; nevertheless, the 2 sets of pathways had extensively overlapping weight distributions. Repeat injections across individuals revealed modest FLNe variability given the range of FLNe values (standard deviation <1 log unit, range 5 log units). The connectivity profile for each area conformed to a lognormal distribution, where a majority of projections are moderate or weak in strength. In the $G_{29 \times 29}$ interareal subgraph, two-thirds of the connections that can exist do exist. Analysis of the smallest set of areas that collects links from all 91 nodes of the $G_{29 \times 91}$ subgraph (dominating set analysis) confirms the dense (66%) structure of the cortical matrix. The $G_{29 \times 29}$ subgraph suggests an unexpectedly high incidence of unidirectional links. The directed and weighted $G_{29 \times 91}$ connectivity matrix for the macaque will be valuable for comparison with connectivity analyses in other species, including humans. It will also inform future modeling studies that explore the regularities of cortical networks.

Keywords: connection, cortex, graph, monkey, network

Introduction

A neurobiological approach to higher brain function, including perception, cognition, and consciousness, must be firmly anchored in a deep understanding of the underlying anatomical circuitry (Koch 2004; Friston 2010). Thus, it is not surprising that understanding the connectivity of cerebral cortex remains a major focus of modern neuroscience (Bohland et al. 2009; Van Essen and Ugurbil 2012).

Large-scale brain networks can be characterized at multiple levels of organization (Bressler and Menon 2010). Here, our level of enquiry is that of the cortical area. Localization of function in the cerebral cortex is closely linked to the concept of the cortical area and is central to our system-level understanding of the neurobiology of the cerebral cortex (Rakic 1988; Mountcastle 1997; Schüz and Miller 2002; Rosa and Tweedale 2005; Zeki 2005). The pathways linking cortical areas have been partially elucidated by numerous anterograde and retrograde tracing experiments that have collectively revealed a number of important organizational principles (Zeki and Shipp 1988; Boussaoud et al. 1990; Felleman and Van Essen 1991; Young 1992; Goodhill et al. 1995; Barbas and Rempel-Clower 1997; Rockland 1997; Jouve et al. 1998; Sporns et al. 2000; Kaas and Collins 2001; Vezoli et al. 2004; Aflalo and Graziano 2011).

Because the patterns of connections between cortical areas are so complex, graph theoretic approaches offer a valuable way to explore their network properties (Watts and Strogatz 1998; Barabasi and Albert 1999; Watts 1999; Newman 2003; Boccaletti et al. 2006). Just as with many other real-world networks (Boccaletti et al. 2006), cortico-cortical connections are directed as well as weighted. Here, we investigated both of these features in order to elucidate the specificity of cortical projection patterns. These results provide valuable information and constraints for future models of cortical networks.

An early systematic study compiled the interareal connectivity of 32 visual areas in the macaque (Felleman and Van Essen 1991). In the resultant 32 × 32 connectivity matrix, these authors reported 305 known projections out of 992 possible pathways, giving a link density (or graph density) of 32% for the visual cortex, that is, one-third of the maximum possible connections among visual areas were reported to exist. Subsequent studies using improved tracers, more systematic methods, and different parcellation schemes revealed numerous additional pathways. For example, the number of reported connections of areas V1 and V2 expanded from a half-dozen (Felleman and Van Essen 1991) to 20 inputs to V1 and 16 to V2 (Boussaoud et al. 1990, 1991; Felleman and Van Essen 1991; Rockland and Van Hoesen 1994; Rockland et al. 1994; Stepniewska and Kaas 1996; Felleman et al. 1997; Barone et al. 2000; Falchier et al. 2002; Clavagnier et al. 2004; Gattass et al. 2005).

While it is well known that cortico-cortical pathways vary widely in their weight (connection strength), surprisingly little data are available on quantitative connectivity profiles in nonhuman primates (Falchier et al. 2002; Barbas et al. 2005; Burman et al. 2011; Markov et al. 2011). For example, the

distribution of retrogradely labeled neurons from selected injections in the macaque parietal cortex (Lewis and Van Essen 2000) was converted into maps of labeled neuronal density (Van Essen et al. 2005), but not into quantitative estimates of interareal connection weights. Likewise, there has been little quantitative data on the weight consistency of any given pathway. A seminal paper analyzed data across studies and concluded that between-animal variability of a given pathway can exceed 2 orders of magnitude (Scannell et al. 2000). In contrast, a recent hemisphere-wide analysis involving retrograde tracers injected into areas V1, V2, and V4 showed greater consistency, with interindividual variability typically less than an order of magnitude (Markov et al. 2011). The latter study also identified many newly found projections (NFP), especially with areas outside the classical visual system. Here, we apply similar sampling procedures and statistical methods in an analysis of connectivity profiles for 29 cortical areas, thereby providing a quantitative connectivity database of unprecedented scope and detail.

Previous studies reported that the vast majority of pathways between cortical areas are reciprocal. Felleman and Van Essen (1991) identified only 5 unidirectional pathways out of the 126 explicitly tested pairs. In contrast, our analysis of a 29×29 subset of cortical areas indicates an unexpectedly high incidence of unidirectional (nonreciprocal) pathways.

Many existing network models assume that the network is sparse, that is, only a small fraction of all possible interareal connections actually exist (Watts and Strogatz 1998; Sporns and Zwi 2004; Honey et al. 2007; Hagmann et al. 2008). By demonstrating that the density of the binary cortical graph (i.e. present vs. absent) is much higher than previous estimates, we provide important constraints on the classes of theoretical networks that are relevant to modeling interareal connectivity.

The growing efforts to explore large-scale models of cortical connectivity (Honey et al. 2007; Sporns et al. 2007; Rubinov and Sporns 2010; Adachi et al. 2012) are hindered by the fact that available databases have been collated from multiple studies using different methods of tracing, nonmatching areas, nomenclature and planes of section, and at best only a qualitative assessment of connection weights (Felleman and Van Essen 1991; Stephan et al. 2001; Kotter 2004). Here, we report on a large-scale anatomical investigation of the macaque cortex, employing retrograde tract tracing using identical protocols and a high-resolution analysis. This enabled us to construct an extensive and quantitative database of the weights and directions of interareal connections using a standardized parcellation scheme. Injections were made in 29 target areas (4 in occipital, 6 in parietal, 6 in temporal, 5 in frontal, 7 in prefrontal, and 1 in limbic regions). The pattern of source areas for each injection was determined using a parcellation of the entire cortical sheet into 91 architectonic areas drawn from published atlases (Paxinos et al. 2000; Saleem and Logothetis 2007) and other studies. The values for the resultant connectivity profiles depend, of course, on our choice of this parcellation scheme, rather than any of the numerous alternative macaque cortical parcellations that are in common use (Van Essen et al. 2005; Van Essen, Glasser, Dierker, Harwell 2011). However, we believe that use of an alternative parcellation would have had little effect on our main conclusion (see the Discussion section).

Our previous analysis of the connectivity profiles of early visual areas, based on statistical properties of extrinsic fraction of labeled neurons (FLNe) values (see the Materials and Methods section), included 2 important findings (Markov et al. 2011). 1) For repeat injections of the same area, the distribution of FLNe values could be modeled as a negative binomial, in which the dispersion parameter determines the relation between the observed mean in FLN values and its variance. 2) The FLNe values of individual connectivity profiles followed a lognormal distribution, in which a majority of interareal pathways have moderate or sparse connection weights. Here, we demonstrate that both features, the negative binomial and lognormal distributions, generalize to other cortical areas and evidently reflect important regularities of neocortical organization. These regularities are important because they provide an empirical framework for interpreting the results from single injections into other cortical areas.

Our analysis of 1615 connections, including 36% that we consider to be NFP, reveals a high density of cortico-cortical connectivity (66%) and an unexpectedly high incidence (33%) of potentially unidirectional pathways, of which one-third (10% of the total) were shown to originate from corresponding locations within the connected cortical areas. The NFP make an important contribution to the connectivity profile of each area. These findings have important consequences for understanding cortical physiology and large-scale models of the cortex.

The present findings provide a unique and valuable dataset that will aid in interpreting neuroimaging-based connectivity studies in humans as well as nonhuman primates. Indirect methods of assessing cortical connectivity using diffusion imaging and resting state functional connectivity are insensitive to the direction of connections and are limited in estimating the weight of the underlying anatomical connections (Hagmann et al. 2008). Such data can only be obtained in animal models using invasive pathway-tracing methods of the type used here, which enable quantification of connectivity with single-neuron level resolution.

Materials and Methods

Single injections of fluorescent retrograde tracers, fast blue (FsB) and diamidino yellow (DY), were made in 28 macaque monkeys (27 *Macaca fascicularis* and *1 Macaca mulatta*). Surgical and histology procedures were in accordance with European requirements 86/609/EEC and approved by the competent veterinary and ethical services. Detailed description of these methods is given elsewhere and further information is provided in the Supplementary material (Markov et al. 2011). Since we use retrograde tracers, the injected area is referred to as the target area and the area containing labeled neurons as the source area. After appropriate survival times and histological processing, high precision maps of neuron location were made using the software package Mercator running on ExploraNova® technology coupled to a fluorescent microscope stage (D-filter set 355–425 nm). Controlled high-frequency sampling allows stable neuron counts, despite the curvature of the cortex and the heterogeneity of neuron distribution in the projection zone (Batardiere et al. 1998; Vezoli et al. 2004) (see Supplementary Fig. 7). Complete scanning of the hemisphere made it possible to determine the full set of ipsilateral cortical source areas projecting to each injected area.

Localization of injection sites and labeled neurons was based on a new reference atlas that includes 91 cortical areas mapped to the left hemisphere of case M132. The atlas parcellation was based on a combination of histological criteria (Markov et al. 2011) and atlas-based landmarks (Paxinos et al. 2000; Saleem and Logothetis 2007) (see Supplementary material for further details). Figure 1*A* shows that this parcellation displayed on medial and lateral views of the M132 left hemisphere surface, generated from contours running through the

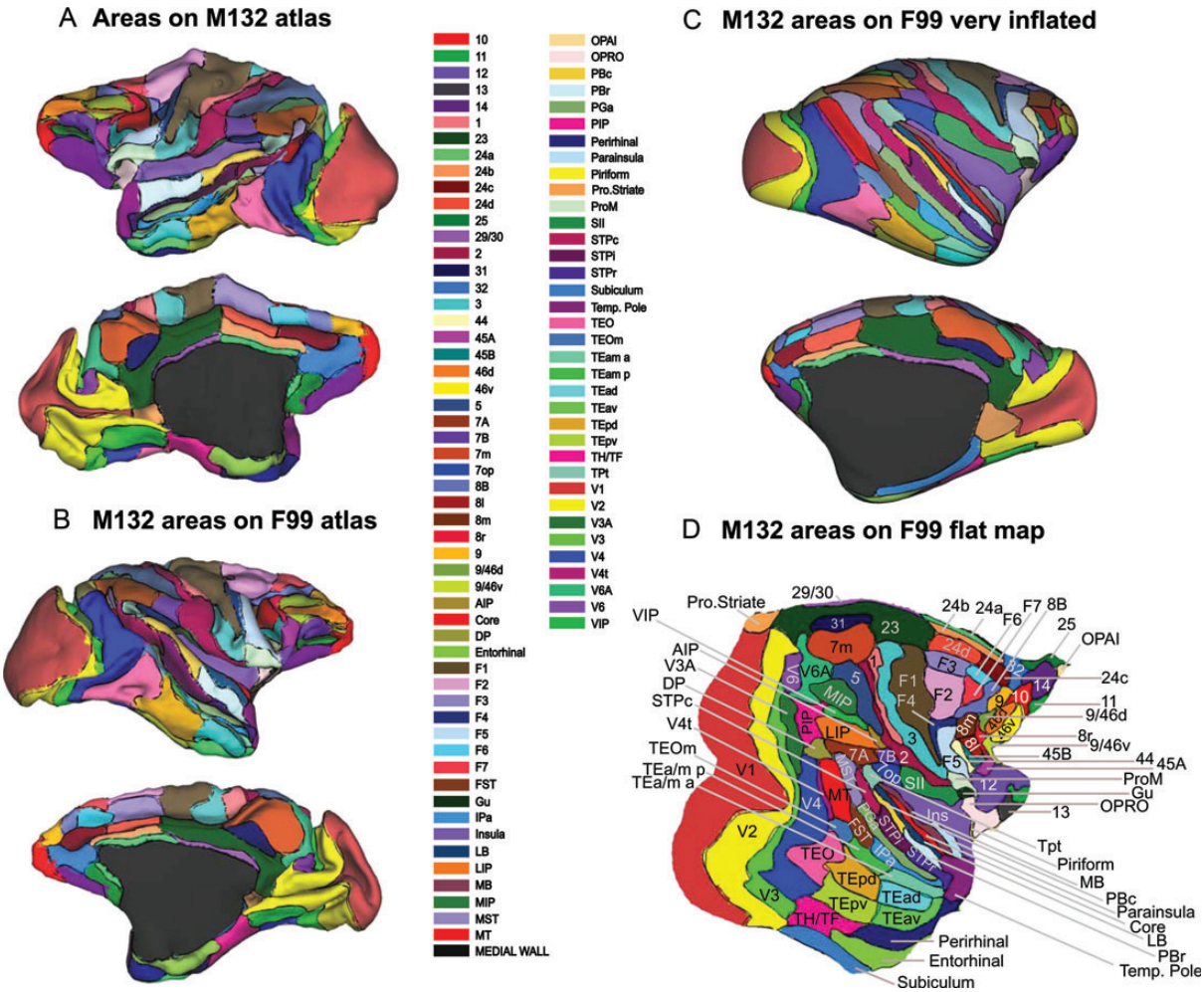

Figure 1. Surface atlas 3D reconstruction. (*A*) The 91 areas of the left hemisphere of M132 reconstructed from section drawings (see Supplementary Fig. 7). (*B*) Lateral and medial views of the 3D anatomical surface displaying areas of M132 transposed on the F99 reference brain medial and lateral view. (*C*) Inflated F99 right hemisphere surface, displaying the M132 areas registered to it. (*D*) F99 flat map with representation of the areas of M132. Criteria for parcellation are given in the Materials and Methods section.

cortical midthickness (approximately layer 4). Figure 1*B–D* shows the same parcellation after landmark-based surface registration to the macaque F99 atlas, displayed on a midthickness, inflated, and flat map surfaces (Van Essen 2004; Van Essen, Glasser, Dierker, Harwell 2011). Section contours for the complete atlas parcellation are shown in Supplementary Figure 7.

Quantification of Connection Weights and Identification of NFP

Briefly, brains were sectioned (40 μm thickness) and 1 in 3 sections retained for analysis. Importantly, when exploring for labeled neurons, 1 section in 2 (i.e. at 240 μm intervals) was examined throughout the cortical gray matter, which enabled the identification of many NFP. However, not all sections were scored when mapping heavily labeled areas. For details on bookkeeping of connectivity values, see Supplementary Materials and Methods. Areal boundaries on individual cases were assigned primarily using gyral and sulcal landmarks relative to the atlas with recourse to histological criteria when required (see Supplementary material). So as to derive the total number of labeled neurons for each pathway (see Supplementary Table 3), we used the observed counts generated by the frequency employed to estimate the expected number of neurons for 1 in 3 sections reserved for counting. This procedure facilitates using different sampling frequencies for areas with very high and very low cell counts. Hence, the number of neurons reported in Supplementary Table 3 corresponds to about one-third of the expected number in the brain for a given injection. The uptake zones of each injection site correspond to a small fraction of the area injected; the volumes of the uptake zone are given in Supplementary Table 2. Injection sites were in general restricted to the cortical gray matter (see Supplementary Fig. 6). However, in areas V1 (section 180), V4 (section 154), TEO (sections 187 and 195), 8m (section 161), 10 (section 20), and 7m (section 340), there was minor encroachment into the white matter (see Supplementary Fig. 6). This may have led to some contamination by fibers of passage, but we consider this unlikely to be a major confound (see the Discussion section).

For each injection, the number of labeled neurons in a given source area relative to the total number of labeled neurons in the brain (including those in the injected area) defines the FLN of the source area (Falchier et al. 2002; Markov et al. 2011). The FLNe of an area is estimated from the number of labeled neurons in that area relative to the total number of labeled neurons less the neurons intrinsic to the injected area. For some analyses, connections are reported as strong ($\log_{10}$(FLNe) greater than −2), moderate ($\log_{10}$(FLNe) equal or less than −2 and greater or equal to −4), or sparse ($\log_{10}$(FLNe) less than −4).

To identify connections to the 29 target areas that were not previously reported, we assessed the connections reported in 119

published studies of connectivity (see Supplementary Tables 1 and 6). We adopted a conservative position with regard to categorizing the NFP. In some publications, connections that we report as known were illustrated but not explicitly listed in the text of the publication. Many such connections are not represented in existing databases. Here, only projections that previously were neither depicted nor listed in publications or databases (cf. see Supplementary Tables 1 and 6) are classified as NFP. The veracity of labeled neurons were checked by senior team members (H.K., C.D., P.M., N.T.M., and C.L.).

Modeling Inconsistency

It is critical to evaluate the reliability of observing a given connection across multiple injections. We refer to this as the consistency of a connection or pattern of connections. Repeated injections into areas V1, V2, V4, and 10 were used to assess the consistency of projections to the early visual areas and a representative prefrontal area. In our previous study, the negative binomial model provided a good description of the variability of the mean counts of the inputs to the early visual areas (Markov et al. 2011). Using identical methods to evaluate the data from the area 10 injections, we confirmed that area 10 is also well described by the same negative binominal model. By extension, we assume that a negative binomial model with similar dispersion should be valid for injections in other regions. For a negative binomial distribution with a known dispersion, there is a functional relation between the variance and the mean, that is, the variance of the negative binomial distribution is $\mu+\mu^2/\theta$, where μ is the mean and θ the dispersion. We used this relation in order to estimate the precision of projections from individual injections as well as to model the consistency of the sparse connections.

To analyze statistical characteristics of inconsistent projections, we calculated the probabilities of observing no neurons under several models. For the simple case of the Poisson distributed counts, the probability of observing y counts given the mean number of counts, μ, is:

$$P(y|\mu) = \frac{e^{-\mu}\mu^y}{y!}$$

For $y = 0$,

$$P(y = 0|\mu) = e^{-\mu} \quad (1)$$

For the negative binomial distribution, the probability density is:

$$P(y|\mu, \theta) = \frac{\Gamma(y+\theta)}{\Gamma(\theta)\Gamma(y+1)}\left(\frac{\theta}{\theta+\mu}\right)^{\theta}\left(\frac{\mu}{\theta+\mu}\right)^{y}$$

where Γ is the gamma function and θ the dispersion. Then, the probability of observing zero counts is

$$P(y = 0|\mu, \theta) = \left(\frac{\theta}{\theta+\mu}\right)^{\theta} \quad (2)$$

For the special case of the geometric distribution ($\theta = 1$), the probability of zero counts is:

$$P(y = 0|\mu, \theta) = \left(\frac{1}{1+\mu}\right) \quad (3)$$

Let p be the probability of observing zero counts from a projection from a single injection, as given by any of equations (1)–(3). The probability of observing at least one or more neurons in a projection (i.e. $y > 0$) from a single injection is $1-p$. Since each injection is independent, the probability that some neurons are observed in each of n injections, is $(1-p)^n$, and the probability of observing no neurons in at least 1 of n injections is $1-(1-p)^n$. This represents the probability of observing zero counts in one or more of the n injection experiments performed.

Updates, atlases, and additional information are available at www.core-nets.org. Surface-based atlas datasets are accessible at http://sumsdb.wustl.edu/sums/directory.do?id=8287442&dir_name=MARKOV_CC12.

Results

Injections were included in our analysis if they showed little or no involvement of the underlying white matter and were restricted to a single cortical area. The extent of each injection relative to areal borders and white matter is shown in line drawings of selected section contours for each individual case in Supplementary Figure 6. The full set of 39 injections in 29 areas after mapping to the atlas surface is shown in Supplementary Figure 1. This mapping provides each injection site with a well-defined stereotaxic location that is independent of the underlying cortical parcellation for the stereotaxic coordinates of the injection sites (see Supplementary Table 7). Hence, while the focus of our analysis is on the pattern of area-to-area connectivity, these data can also be evaluated in terms of the areal inputs to a set of atlas coordinates that have well-defined locations relative to alternative parcellation schemes that have been mapped to the F99 atlas (Van Essen, Glasser, Dierker, Harwell 2011; see the Discussion section).

We first show how modeling the observed variability of FLNe in repeat injections allows the estimation of the reliability of results obtained from a single injection. One important question is how closely the weight of a pathway observed after a single injection approximates the average connection weight determined from repeat injections. A second issue concerns the consistency of connections. If a given interareal pathway is observed after a single injection, what is the likelihood that the same pathway will be observed after repeat injections, and to what extent does this likelihood depend on the observed connection weight (FLNe)? To address these issues, we extended our previous analysis of connectivity variability for visual areas V1, V2, and V4 (Markov et al. 2011) to include prefrontal area 10, which (as shown below) is more extensively connected than are early visual areas and might in principle show different variability dependencies.

Modeling Variability of FLNe Values in Area 10

Repeat injections were aimed at area 10 at the very rostral tip of the cortex. Figure 2 shows four 3D views of each reconstructed injection site in relation to the pial surface (gray) and the gray/white border (blue). Inspection of these reconstructions, especially the medial views (far right column), confirms that the uptake zones were restricted to the frontal pole, spanning the cortical gray matter but not encroaching on the underlying white matter (see Markov et al. 2011 for details on uptake zone determination). The 2 smallest injections (M131LH and BB341LH, Fig. 2*A*,*D*) had almost identical locations in the rostral pole. The 2 larger injections (M136LH and M137LH, Fig. 2*B*,*C*) also included the anterior pole but extended further ventro-laterally.

The 4 repeat injections in area 10 showed similar labeling connectivity profiles in terms of the identity of labeled areas and the FLNe values for each projection. In Figure 3*A*, the log (FLNe) values are ordered by the geometric means of neuron counts (thin red line) for all areas that project to area 10 in one or more cases. Fifteen projections had a mean FLNe value exceeding 10^{-2}, which we classify as a strong projection.

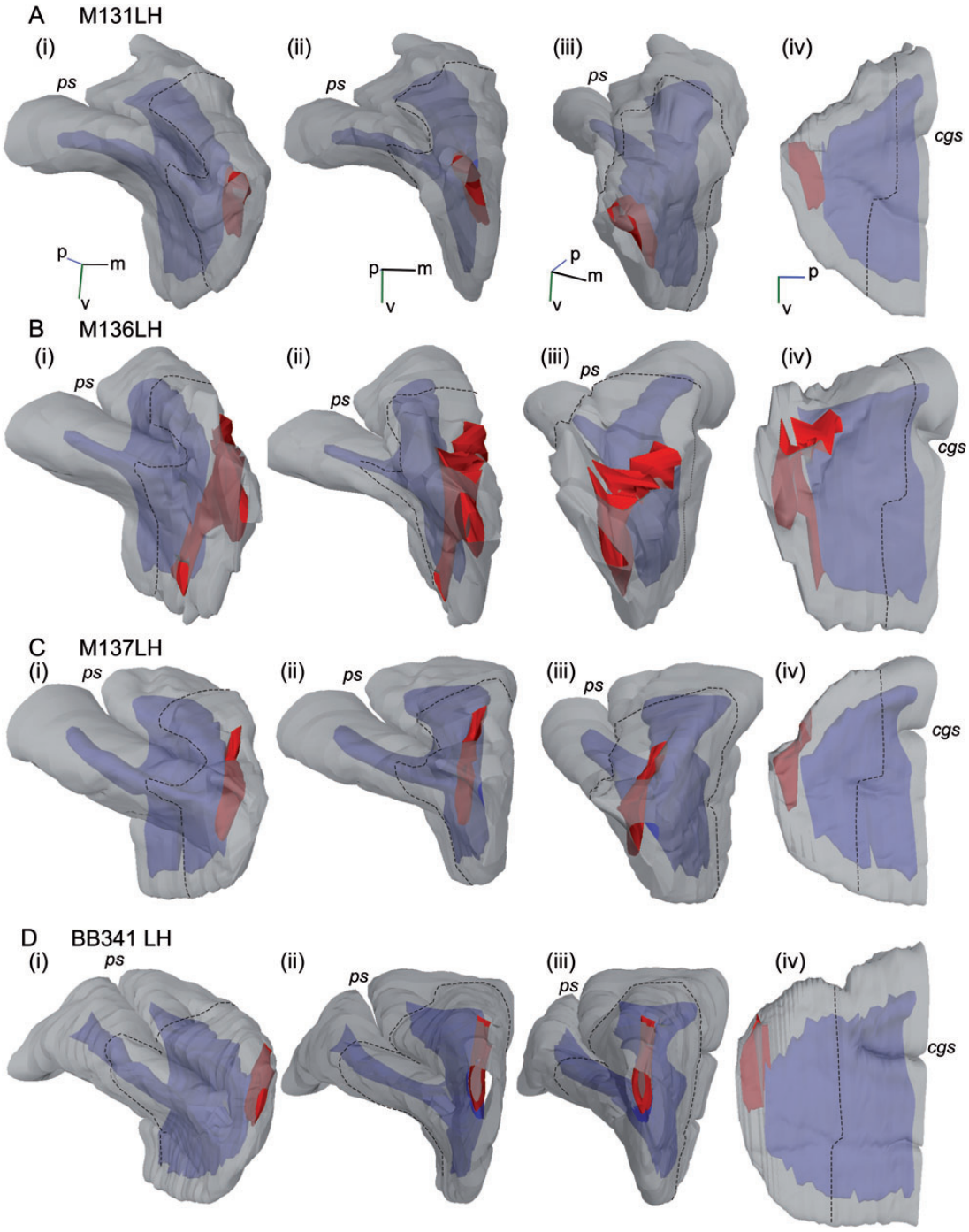

Figure 2. Three-dimensional reconstruction of the 4 injection sites in area 10 (respectively, cases 34, 37, 38, and 39). Injection site in red and white matter in blue. Dotted line shows the limits of area 10. (i) Fronto-lateral view, (ii) frontal view, (iii) fronto-medial view, and (iv) medial view.

Twenty-seven projections had FLNe values between 10^{-2} and 10^{-4}, which we classify as moderate in strength. Twenty-four projections had FLNe values below 10^{-4}, which we classify as sparse. The geometric mean is reasonably well fit by a lognormal distribution (thick black line), as previously observed for visual areas V1, V2, and V4 (Markov et al. 2011).

The observed range of FLNe values for the 4 repeat injections in area 10 is less than one order of magnitude for most areas. However, for 4 input areas (45A, 31, 7A, and DP) the range exceeds 2 orders of magnitude. In Figure 3*B*, the standard deviation (SD) and mean is fit by a negative binomial distribution (green line) having a dispersion parameter of 5.0 (see the Methods section). The best-fitting negative binomial curve differs considerably from a Poisson distribution (red line) except for low FLNe values. It is closer to a geometric distribution (blue line), as was seen for injections of areas V1, V2, and V4 (Markov et al. 2011). The dispersion parameter obtained from area 10 (5.0) yields a curve similar to that obtained from the visual areas (average dispersion, 7.6).

Some of the observed variability might be attributable to measurement errors owing to imperfect delineation of areal boundaries for the various source areas. One way to assess

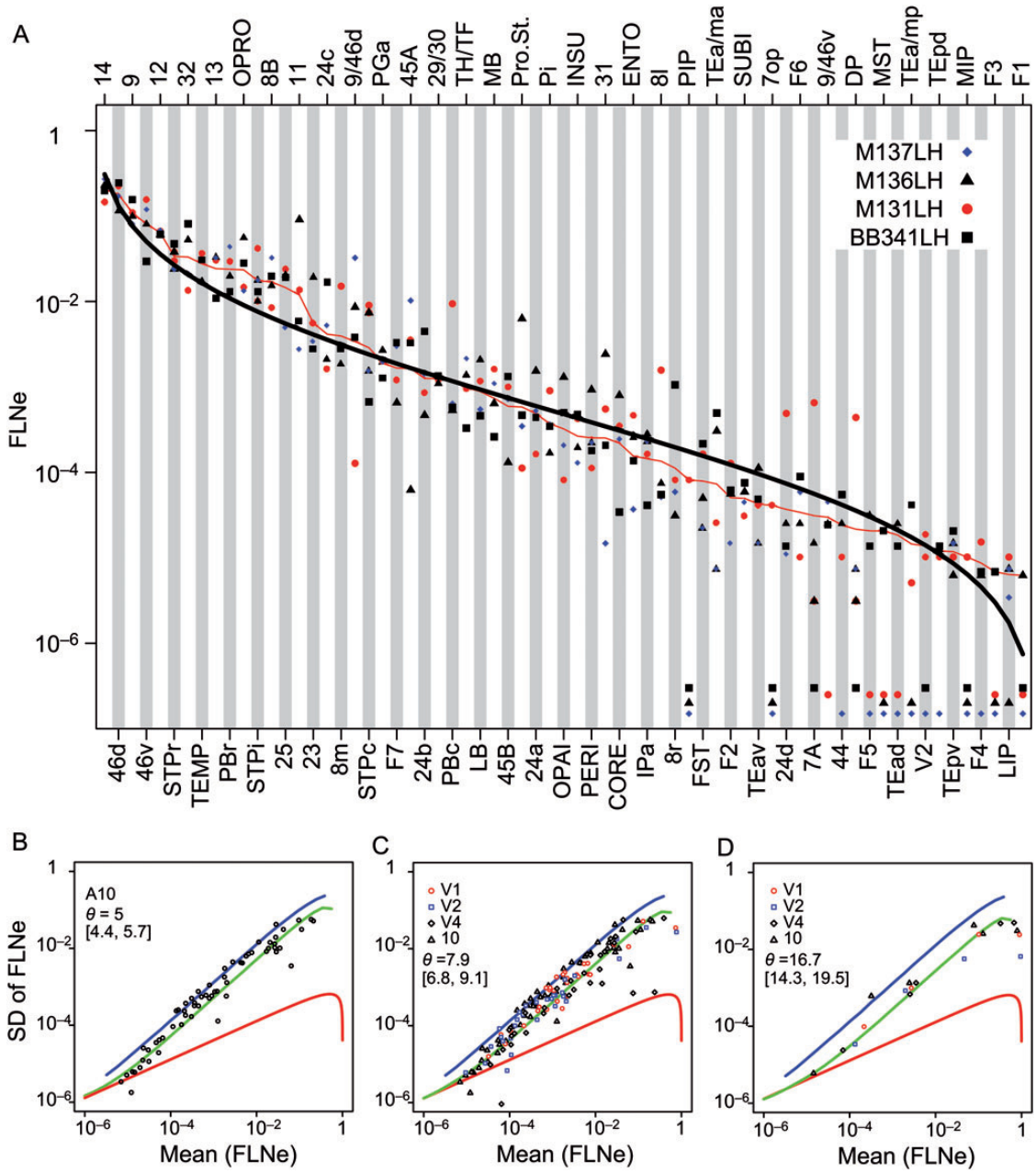

Figure 3. Variability of labeling after repeat injections in area 10. (*A*) FLNe plotted by area for 4 injections in cortical area 10 ordered by the geometric mean (thin red curve) of the values for each projection (excluding data points for "absent" projections when computing the mean). The thick black curve indicates the expected values for an ordered sample from a lognormal distribution with the same mean and SD. Symbols below 10^{-6} indicate zero values. (*B–D*) The SD as a function of the mean. The curves are the predictions for a Poisson (red), geometric (blue), and the best-fitting negative binomial distribution (green). The dispersion parameter of the negative binomial distribution and its 95% confidence interval are indicated in the inset; (*B*) values for the 4 injections in area 10; (*C*) areal values for the repeat injections in V1, V2, V4, and area 10; (*D*) cumulative regional values.

variability due to errors in the location of area borders is to compare the variability of the repeat injections in areas V1, V2, V4, and 10 (Fig. 3*C*) with the variability observed when the areas are grouped into much larger regions (Fig. 3*D*). Comparisons of the slopes in Figure 3*C*,*D* show only a modest reduction in variability, suggesting that areal delineation is not the major source of variability.

In terms of the presence versus absence of connections, the 4 repeat injections in area 10 showed similar labeling patterns (Fig. 3*A*). For the 67 areas containing label from at least one injection, 50 (75%) were labeled by all 4 injections, 7 by 3 injections, 4 by 2 injections and 6 by only a single injection; 24 areas lacked connections to the injection area in all 4 cases. Of the 17 areas labeled by fewer than 4 injections, 15 were very sparse, with labeling of fewer than 10 neurons on average. These were near the limit of systematic detectability expected for a variable where the heteroscedasticity of the SD/mean relation follows a negative binomial distribution (Fig. 3*B*). The 2 exceptions were areas 7A and DP, with moderate labeling following a single injection.

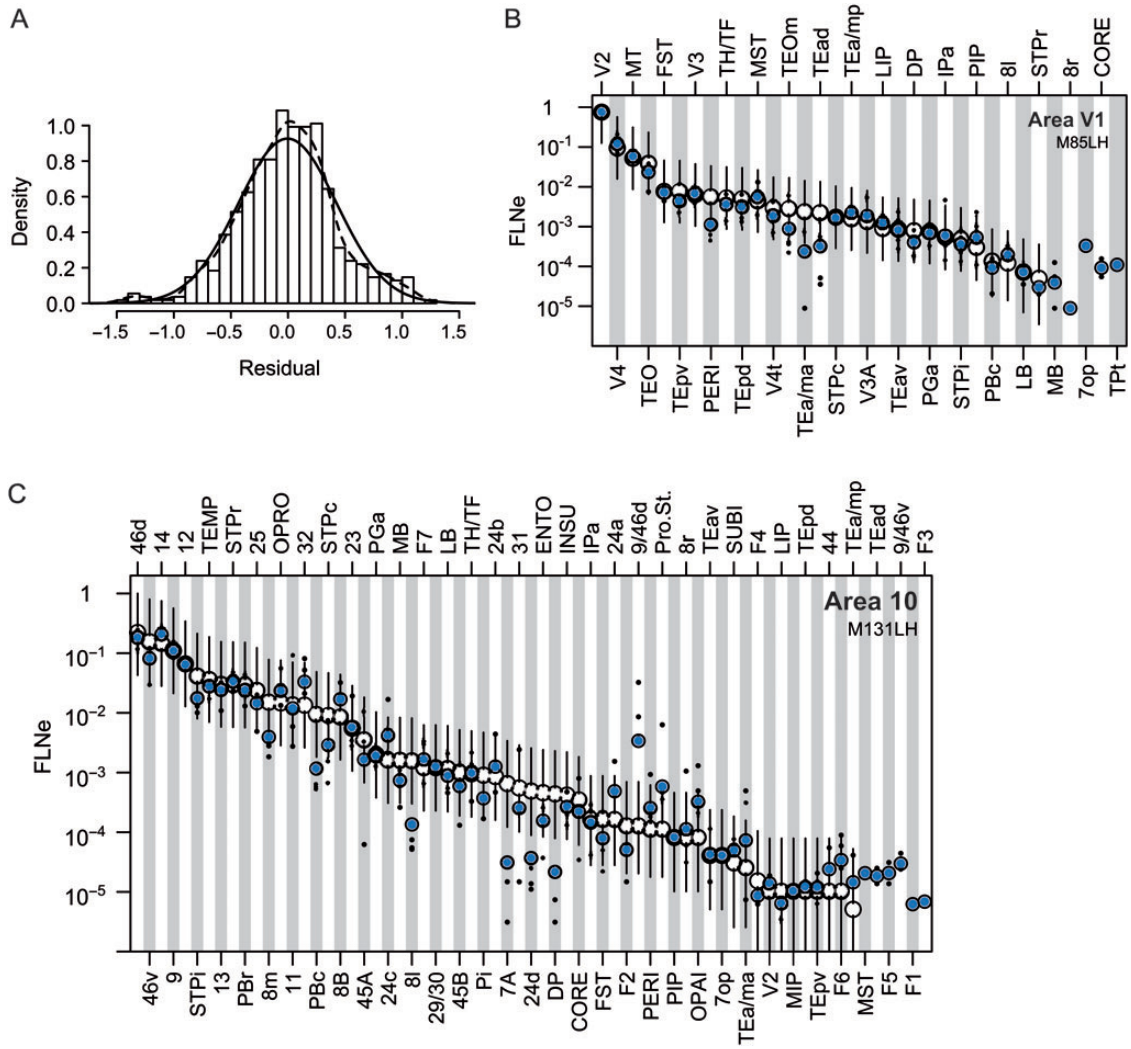

Figure 4. Relationships of means and 95% confidence intervals from multiple injections to the values from single injections. (*A*) Histogram of residuals for multiple injections (V1, V2, V4, and 10) with respect to lognormal order statistics normalized to unit area. Dashed curve: A kernel density estimate of the underlying distribution obtained by convolution of the histogram with a Gaussian; solid curve: Best-fitting normal distribution (mean = −0.003, SD = 0.430). (*B*) Ordered FLNe values from a single injection in cortical area V1 (white circles) with 95% confidence intervals expected on the basis of a negative binomial distribution (error bars). The small black dots correspond to values obtained from 4 other injections in the same area. The blue circles are the geometric means. For the 3 entries on the far right (MB, 8r, and 7op), there were no labeled neurons from the V1 injection used for FLNe rank ordering. (*C*) Ordered FLNe values from a single injection in cortical area 10 (white circles) with confidence intervals and small black dots (3 other injections) and blue circles as described for area V1. For the 8 entries on the far right, there were no labeled neurons from the area 10 injection used for FLNe rank ordering.

Using Single-Injection FLNe Values to Predict the Mean from Multiple Injections

For the multiple injections in V1, V2, V4, and area 10, the histogram in Figure 4*A* shows the residual between the log (FLNe) values from individual injections and the predicted lognormal curve. This provides a quantitative measure of the relationship between average connection weights and the values obtained from individual injections. Given an FLNe value from only a single injection, the mean value (i.e. the value for the lognormal distribution) lies within a factor of 2.7 (1 SD) in about 68% of cases. The observed variability presumably reflects a combination of factors (see the Discussion section).

The analysis illustrated in Figure 4*B*,*C* and Supplementary Figure 3 indicates how accurately FLNe values from a single injection can predict the mean obtained from multiple injections. Figure 4*B* shows the ordered FLNe values from a single V1 injection (white circles), with a 95% confidence interval assuming a negative binomial distribution analysis with the dispersion observed following the multiple injections. The difference between the observed single-case value and the mean of 5 injections (blue circles) is generally quite small and for this exemplar injection in every case lies within the 95% confidence interval predicted by the negative binomial distribution. The maximum difference is 0.99 log unit, corresponding to a 9.5-fold difference between the single-subject and group-average results. A similar analysis for area 10 (Fig. 4*C*) shows a comparably good fit for most of the data involving strong and moderate projections. However, for a few projections, the difference between individual and group average exceeds an order of magnitude. For the full set of 14 repeats (see Supplementary Fig. 3), involving 544 single FLNe values, the 95% confidence values included 98.5% of the observed FLNe means determined from repeat injections. Altogether, this analysis indicates that FLNe values obtained

from single injections are usually within a factor of 3 and highly likely to be within a factor of 10 of the mean value. However, exceptions can occur, especially for sparse connections, as discussed in the next section.

Consistency of Sparse Connections

Elsewhere we have shown that increasing the sampling rate reduces the variability in estimates of the FLNe (Vezoli et al. 2004). Here, we consider how sampling rates influence the consistency.

For the 37 projections having interpolated mean counts fewer than 10 neurons, 31 were inconsistent (see Supplementary Table 3). Here, we want to distinguish between inconsistency attributable to sampling error (e.g. due to incomplete sampling given that not all sections were examined) and genuine biological variability in which some pathways are present in some but not all cases. The following analysis indicates that statistical fluctuation due to sampling errors can largely account for the observed inconsistency of very sparse projections.

Figure 5*A* shows the probability of observing zero counts (i.e. failing to detect a connection that exists, namely a false-negative) as a function of the mean (expected) number of labeled neurons, μ, after a single tracer injection for Poisson, negative binomial, and geometric distributions (eqs 1, 2, and 3, respectively, in the Materials and Methods section). The probability of a false-negative falls below 0.05 (grey horizontal line in Fig. 5*A*) for means as low as 4 neurons for both the negative binomial and Poisson curves, consistent with the convergence of their variance/mean ratio at small FLNe values shown in Figure 3*B*. The probability of observing at least one false-negative decreases is a sigmoid function of the mean, as shown in Figure 5*B* for 2, 3, and 5 injections (spanning the range in our data set). For 5 repeat injections, as in our V1 injections, the false-negative probability falls below 0.05 (grey horizontal line) for a mean of 7 neurons. The probability of observing at least one false-negative after 5 injections drops much more steeply for a negative binomial than for a geometric distribution (Fig. 5*C*).

Taking the observed mean as the best estimate of the population mean (or expected value), the probability of the observed inconsistency under the negative binomial model exceeds 0.05 for 27 of 39 projections having an observed mean fewer than 10 neurons (see Supplementary Table 3, column G). Of the 12 cases with probabilities below 0.05, 3 are consistent and had an observed mean exceeding 7 neurons. After applying the Bonferroni correction for evaluating multiple probabilities (Bretz et al. 2010), only the projections of areas 7A and DP to area 10 were inconsistent despite a statistically very low probability of being so. Genuine biological variability presumably exists in the connectivity profiles for different individuals, and it is possible that some pathways are present in some individuals and altogether absent in others. However, statistical fluctuations in the data largely accounts for the observed inconsistency of very sparse projections (see the Discussion section). These observations on inconsistency depend on the fine sampling that we employed. In simulations of sparse projections having a negative binomial distribution, coarser sampling had little effect on the expected proportion of zero counts observed, but the variability in the estimates was proportional to the square root of the sampling interval (e.g. a 1:16 sampling interval results in 4 times as much variability in the estimated occurrence of zero counts compared with a 1:1 sampling).

In summary, this analysis of repeat injections provides objective constraints on what can and cannot be learned from making a single injection into any given cortical area. Specifically, a single-injection approach can 1) detect all but the most sparse projections with high probability, 2) provide a reasonable estimate of the connection weight of each pathway (generally within an order of magnitude), and 3) identify some of the sparse connections that are statistically likely to be inconsistent across multiple injections. Repeat injections enable identification of a few additional sparse projections and also provide better estimates of average connection weights. However, given the paucity of quantitative data on interareal connection weights in the macaque (see the Introduction section), the single-injection results described below have advantages in terms of the overall information gained when applied to a large number of areas.

Connectivity Patterns Revealed by Single Injections

Individual injections made into 25 cortical areas (in addition to areas V1, V2, V4, and 10) provided extensive new

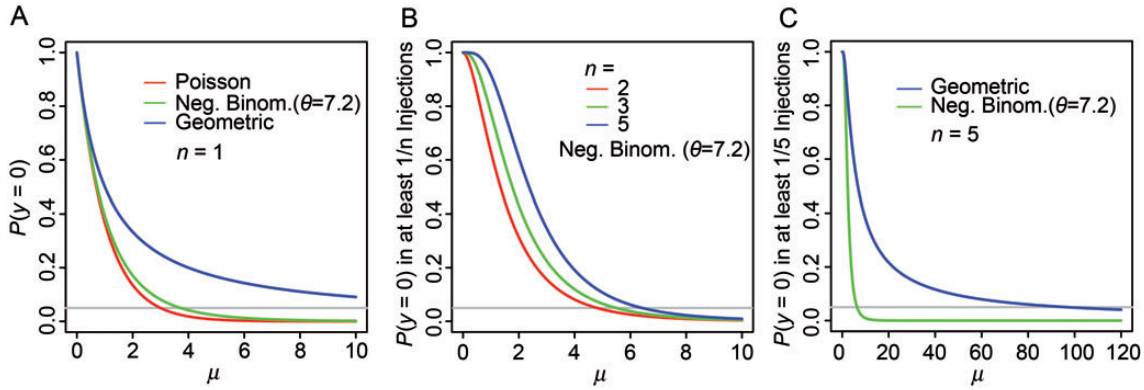

Figure 5. Theoretical analysis of projection consistency. (*A*) Probability of observing zero counts as a function of the true mean for Poisson (red), negative binomial (green), and geometric (blue) distributions. (*B*) Probability of observing at least one case of zero counts in n injections as a function of the true mean for a negative binomial distribution with dispersion parameter equal to 7.2. (*C*) Comparison of the probability of observing at least 1 zero as a function of the true mean in $n = 5$ replications for the geometric (blue) and negative binomial ($\theta = 7.2$) distributions.

information of several different types. This includes the identification of many NFP, quantification of the weight of all pathways (based on FLNe values), demonstration of the lognormal distribution of FLNe values as a general principal of the cortex, and evidence for many unexpectedly unidirectional rather than reciprocal pathways.

We begin by discussing results for an exemplar injection of area F2 in the motor cortex. Figure 6 shows selected section contours with the injection site in solid red, the injected area (F2) in gray, and retrogradely labeled neurons as red dots; labeled neurons intrinsic to the area are not shown. Areal boundaries are indicated by black lines. Source areas representing NFP are labeled in bold blue and marked by an asterisk; the sections were selected to illustrate all the NFP. In a few places, the label in a restricted region (identified by a black rectangle) comes from an adjacent section projected onto the section shown. Red lettering indicates inferred known projections, which although illustrated in previous studies listed in Supplementary Table 6 were not explicitly reported largely due to differences in parcellation scheme used (see below).

Area F2 is located in the dorso-caudal part of Brodmann's premotor area, area 6. It is located anterior to F1 (area 4), extends rostrally up to 3 mm in front of the genu of the arcuate sulcus and is bordered ventrally by the spur of the arcuate sulcus (Matelli et al. 1998). In this case, the injection was dorsal and rostral to the superior precentral dimple (Fig. 6 and see Supplementary Fig. 7) and was in the hind limb representation (Dum and Strick 1991; He et al. 1993; Godschalk et al. 1995; Graziano and Aflalo 2007).

Fifty one projections were identified from this injection, of which 14 we consider NFP. The known projections include 6 areas in the limbic cortex (areas 23, 24a, 24b, 24c, 24d, and 31) (Barbas and Pandya 1987; Ghosh and Gattera 1995; Matelli et al. 1998; Caminiti et al. 1999; Petrides and Pandya 1999; Marconi et al. 2001; Tanne-Gariepy et al. 2002; Luppino et al. 2003; Morecraft et al. 2012), 8 areas in the prefrontal cortex (areas 8B, 8l, 8m, 8r, 44, 46v, 9/46d, and 9/46v) (Barbas and Pandya 1987, 1989; Ghosh and Gattera 1995; Caminiti et al. 1999; Petrides and Pandya 1999; Marconi et al. 2001; Luppino et al. 2003; Takada et al. 2004; Petrides and Pandya 2006; Morecraft et al. 2012), 8 areas in the frontal cortex (areas F1, F3, F4, F5, F6, F7, INSULA, and parainsula) (Barbas and Pandya 1987; Ghosh and Gattera 1995; Caminiti et al. 1999; Petrides and Pandya 1999; Marconi et al. 2001; Tanne-Gariepy et al. 2002; Luppino et al. 2003; Takada et al. 2004; Morecraft et al. 2012), 11 areas in the parietal cortex (areas 3, 5, 7A, 7B, 7m, 7op, AIP, LIP, MIP, VIP, and SII) (Jones et al. 1978; Petrides and Pandya 1984; Ghosh and Gattera 1995; Johnson and Ferraina 1996; Matelli et al. 1998; Caminiti et al. 1999; Cipolloni and Pandya 1999; Petrides and Pandya 1999; Luppino et al. 2001; Marconi et al. 2001; Tanne-Gariepy et al. 2002; Petrides and Pandya 2009; Morecraft et al. 2012), and 4 areas in the temporal cortex (areas MST, STPc, STPi, and TPt) (Seltzer and Pandya 1989; Luppino et al. 2001). Previous evidence for 4 of these projections is relatively sparse: TPt (Luppino et al. 2001), 7op (Ghosh and Gattera 1995; Caminiti et al. 1999; Cipolloni and Pandya 1999), and 9/46v (Takada et al. 2004), so strictly speaking, they could also be considered inferred rather than known.

NFP are located in temporal (9), prefrontal (4), and frontal (1) regions (blue areal labels in Fig. 6). These include area MT (Fig. 6*A*), area MB (Fig. 6*D*), area PERHIRHINAL (Fig. 6*E*), area PBr (Fig. 6*F*), areas IPa, TEa/ma (Fig. 6*G*), area PGa (Fig. 6*H*), area STPr (Fig. 6*I*), area TEMPORAL_POLE (Fig. 6*J*), area ProM (Fig. 6*K*), area OPRO (Fig. 6*L*), area 45B (Fig. 6*M*), and areas 12 and 13 (Fig. 6*N*). These NFP show relatively few labeled neurons in the sections illustrated. Quantification of each pathway (see Supplementary Table 6) indicates that most NFP to F2 are indeed sparse, but several (areas 12, MB, and PGa) are moderate in strength.

Different subregions of F2 have distinct patterns of inputs (Johnson et al. 1996; Matelli et al. 1998; Tanne-Gariepy et al. 2002; Luppino et al. 2003), so it is important to specify the location of the injection site. For example, the injection in case 27 was in the hindlimb representation and did not lead to labeling in areas V6A, 32, and PIP, whereas more lateral and ventral injections (in the arm representation) do label these areas (Johnson et al. 1996; Matelli et al. 1998; Caminiti et al. 1999; Petrides and Pandya 1999; Tanne-Gariepy et al. 2002).

Figure 7 shows a connectivity map for the F2 exemplar injection displayed on cortical surface maps (lateral and medial inflated maps plus a flat map of the F99 atlas). Connection strengths are encoded as sparse, moderate, or strong (dark to light shades) using green for previously reported projections and red for NFP. Several general observations emerge from examination of the F2 connectivity map (Fig. 7) and the other 28 maps (data not shown). In general, the areas providing inputs to any given target area form a group that covers at least half of the cortical surface (e.g. area 24c) and in some cases more than 3 quarters of the hemisphere (e.g. area 7A). The strongest connections tend to be from areas close to the injection, but there are exceptions. NFP are rare in the immediate vicinity of the injected area, but are common at both intermediate and distant locations and often form a near-continuous belt of areas, as in Figure 7.

Weight Distribution of Known Projections and NFP

Injections in all 29 target areas revealed a total of 1,615 cortical pathways. Of these, 579 have not been previously described (NFP). Each target area received projections from between 26 to 87 source areas. Supplementary Figure 2 shows the precise location of injection sites and the pattern of projections in selected section contours for 28 target areas (all but F2). Supplementary Table 6 provides citations for each of the 1,036 known projections reported in this study for all the 29 target areas. The evidence for the existence of the known connections is generally relatively good, insofar as most projections are reported in several studies. The incidence of inferred projections (suggestive but not compelling evidence) described above for area F2 was similar for the other 28 target areas.

For all 29 areas injected, including the 14 repeat injections in 4 areas, we found that the ordered FLNe was well described by a lognormal distribution (Fig. 8 and see Supplementary Fig. 4). The curves in each plot are based only on the mean and SDs of the log10 (FLNe) values and the number of projections; no free parameters were used to constrain the shape of the curves. This consistency in the weight distribution indicates a strong regularity in the cortex. The profiles shown in Figure 8 and Supplementary Figure 4 include 95% confidence intervals based on the negative binomial model fit to the data

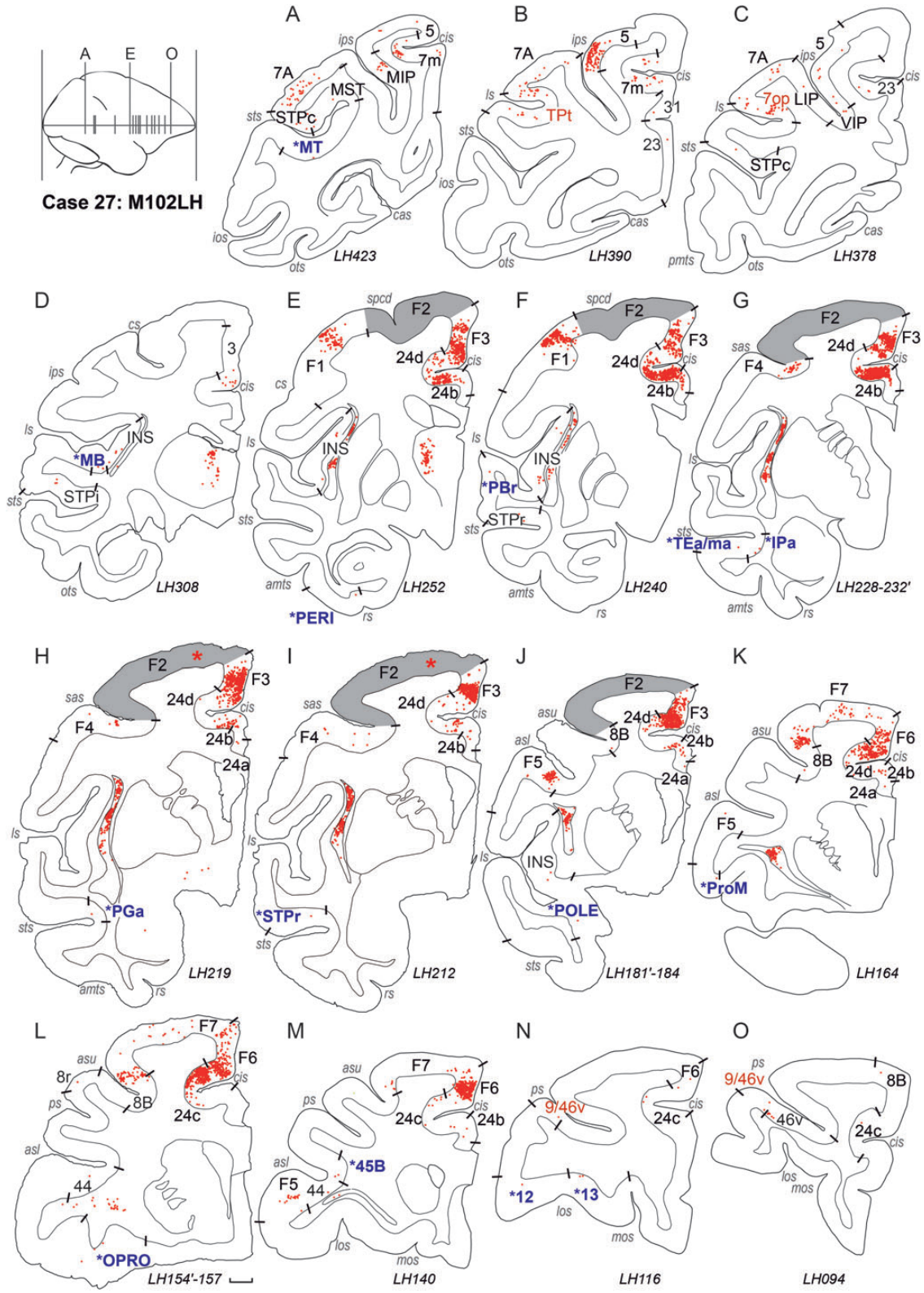

Figure 6. Charts of labeled neurons following injection in area F2. Upper left: Section levels (*A–O*) indicated on a lateral view of the cortex, red filled region indicates pick-up zone of injection site. (*A–O*) Charts of coronal sections of retrogradely labeled neurons (red dots). Black rectangle indicates neurons from nearby sections. Blue lettering and asterisk identifies NFP. Red lettering identifies inferred known projections (see text). Scale bar: 2 mm.

and constitute the connectivity profiles of the 29 injected areas. These curves are necessarily monotonically decreasing by the way they were constructed. However, there is no *a priori* reason why the distribution must be well fit by a lognormal distribution, and we consider this an important experimental finding. The curves shown in Figure 8 illustrate common features in the connectivity profiles including just how closely the single FLNe values track the lognormal

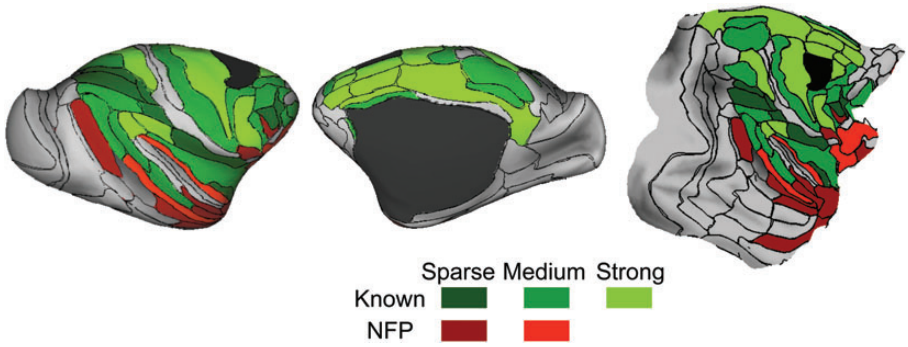

Figure 7. Cortical surface maps for the F2 exemplar injection. Flat map plus medial and lateral inflated maps for injections shown in Figure 8. Connection strengths are encoded as sparse, moderate, or strong (dark to light shades) using green shading for previously reported projections and red for NFP. The area injected is in black.

distribution as well as the progressive widening of the 95% confidence interval with decreasing FLNe values.

Supplementary Table 1 lists the NFP together with the known pathways and supporting publications for each target area. For the target areas in each cortical region, the NFP constituted a substantial fraction of the total number of connections (limbic 13%, prefrontal 40%, frontal 30%, parietal 30%, temporal 43%, and occipital 37%). Figure 9 shows a histogram of connection weights for known projections (white bars) and NFP (red bars) in intervals of 0.5 $\log_{10}$(FLNe). Known connections are on average stronger than NFP, but the 2 populations overlap extensively. Remarkably, 43% of the NFP had FLNe of moderate strength, and a few (2%) are classified as strong connections. For very low FLNe values, NFP correspond up to 90% of the population, but constitute a decreasing fraction of the source areas with increasing FLNe.

Multiway contingency tables make it possible to compare the consistency of NFP and known projections (see Supplementary Fig. 5). This shows that at similar weights, the consistency of the NFP is similar to that of the known projections.

Reciprocity

Connections between any pair of areas can be categorized as bidirectional (reciprocal), unidirectional (a connection observed in only one direction), or unconnected. Previous analyses of this issue have been hampered by the incompleteness of data testing for connectivity in both directions using consistent parcellation criteria (see the Introduction section). The availability of 29 injections analyzed using the same parcellation scheme enabled us to test for the existence of all pathways and to generate an edge-complete graph, which we call $G_{29\times29}$. In our $G_{29\times29}$ edge-complete matrix, the connectivity was bidirectional between 214 projection pairs, unidirectional for 108 pairs, and unconnected for 84 pairs (see Supplementary Table 4). This is a much higher incidence of apparent unidirectional connections than reported in previous analyses (see the Discussion section). Of the 108 unidirectional connections, 4 are classified as strong and 36 as medium (see the Materials and Methods section). For bidirectional connections, we compared the ratio of the FLNe weights for each direction in order to assess the degree of symmetry (see the Materials and Methods section). We categorized 126 reciprocal pathways as symmetric and 88 as asymmetric (see Supplementary Table 4).

As already noted, some cortical areas have nonuniform connectivity across their extent, and this could impact assessments of reciprocity. For example, whereas foveal V1 and V4 are reciprocally connected (Zeki 1978; Zeki 1980; Van Essen et al. 1986), peripheral V4 projects to V1 but does not receive a projection from V1 (Kennedy and Bullier 1985; Perkel et al. 1986). We therefore investigated whether our observation of unidirectional connections may in some cases reflect a misalignment of local connectivity patterns for pathways that are actually bidirectional in an area-to-area sense. Consider a putative unidirectional projection from area X to area Y. We examined the location of labeled neurons in area X (resulting from the injection in area Y) with respect to the injection site in area X (from a different case) that failed to label neurons in area Y. If the injection site of area X overlaps with the labeled neurons projecting to area Y, we consider this strong evidence for a *bona fide* unidirectional pathway. For example, Figure 10*A* shows labeled neurons in area 9/46v following injection in TEO (case 11), and in gray the injection site location in area 9/46v (case 31) that failed to label neurons in TEO. Figure 10*B–E* shows 4 additional examples of overlap between unidirectional projections and the injection site testing the reverse direction. For the 58 out of 108 apparently unidirectional pathways in which more than 10 neurons were labeled, 32 showed an overlap between the injection site and labeled neurons indicative of a genuine unidirectional projection (see Supplementary Table 4). This analysis suggests that a minimum of 10% of the 322 connected pairs are genuinely unidirectional, and over half of these have medium to strong FLNe values (see also the Discussion section).

A 29 × 91 Weighted Connectivity Matrix

Figure 11*A* shows the 29 × 91 connectivity matrix in which the color of each entry represents the log10 (FLNe) value for that pathway (brighter shades representing stronger connection weights; black represents no connection). Each column gives the FLNe profile of inputs observed for a given area and each row its outputs. The matrix is asymmetric, in contrast to many connectivity matrices obtained using neuroimaging methods that cannot distinguish the directionality of connections. The rows and columns were ordered so as to maximize the overall similarity between neighbors (see the Materials and Methods section). Visual areas are concentrated in the upper left quadrant of the matrix. Motor and somatosensory areas are concentrated in the lower right quadrant. Higher-level areas of the frontal, parietal, and temporal cortex are mainly in the middle portion. Green squares indicate the "identity" entry for the same area in a row and column. These entries run approximately along the diagonal, suggesting that areas having a similar pattern of inputs also have a similar

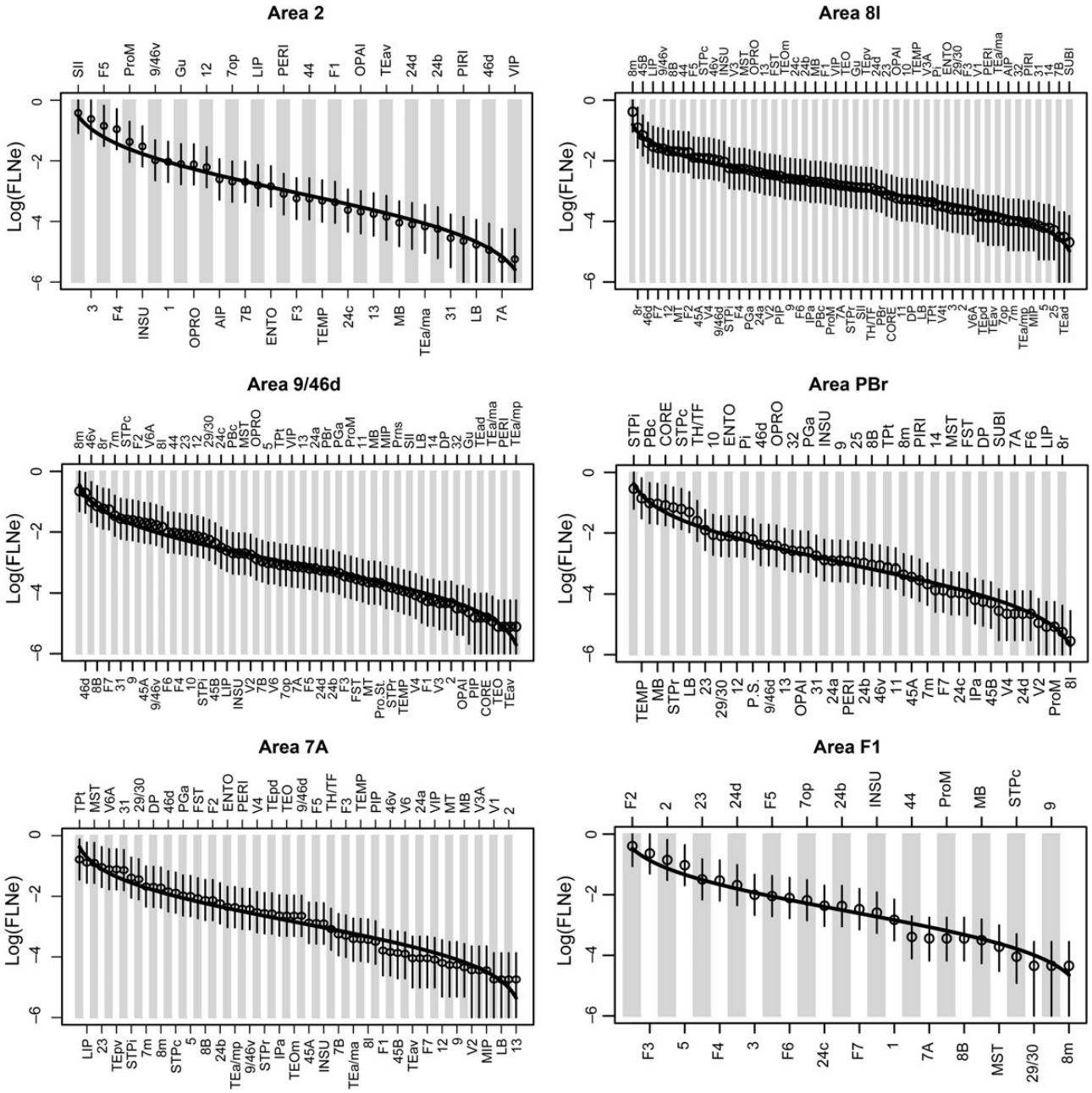

Figure 8. Connectivity profiles for 6 injected areas, chosen to illustrate a greater than 3-fold range in number of connections (in-degree distribution, see Fig. 12). The log(FLNe) values are ordered. The solid curves correspond to the predicted order statistics for a lognormal distribution with the same mean and SD as the data. The error bars are 95% confidence intervals, assuming that the data follow a negative binomial distribution with dispersion equal to 7. Connectivity profiles for the remaining injections are displayed in Supplementary Figure 4.

pattern of outputs. However, the many deviations from the diagonal suggest that some areas having similar input profiles have distinctly different output profiles, and vice versa. Figure 11*B* shows a 29×29 matrix that includes only source areas that also served as injection sites. Deviations from symmetry along the diagonal for black entries signify asymmetries in the existence of observed projections. Deviations from symmetry in the shaded entries signify asymmetries in the strength of these projections.

Graph Density

Existing databases do not provide reliable estimates of the density of the network of cortical areas, nor has there been a concerted effort to extrapolate from the existing data to the connectivity of the full interareal network (FIN). Here, we explore the classical notion of graph density (Janson et al. 2000; Newman 2010) of the FIN using multiple approaches that give converging results. This analysis draws from the weighted connectivity matrix (Fig. 11) using binary measures of connectivity (i.e. connections existing or not, independently of their strength). Graph density is a fundamental measure of the graph's overall connectedness, extensively used in network science and also in earlier analyses of cortical connectivity (Sporns and Zwi 2004; Bullmore and Sporns 2009).

Based on the M132 atlas parcellation (Fig. 1), the FIN contains $N_{\mathrm{FIN}} = 91$ cortical areas that represent the nodes of the

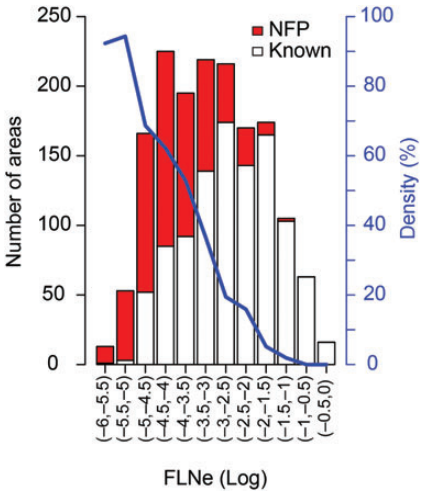

Figure 9. Weight comparisons for known projections and NFP Distribution of known projections and NFP as a function of projection magnitude (FLNe) at intervals of 0.5 $\log_{10}$, following the injection of the 29 target areas. Blue line indicates the percentage of NFP within each interval.

$G_{91\times91}$ graph. The directed edges of the FIN correspond to directed connections between nodes, based on the FLN. Our analysis of the FIN makes use of the $G_{29\times91}$ directed subgraph of projections within FIN, which reveals all the in-degrees of the injected 29 nodes. It also makes use of the $G_{29\times29}$ edge-complete subgraph of FIN, corresponding to the connections among just the 29 injected areas. Both $G_{29\times91}$ and $G_{29\times29}$ contain complete information about the status of their edges and would not be influenced by injections into additional areas elsewhere in the cortex. Given that the 29 injected areas are widely distributed among the 6 regions, the $G_{29\times29}$ subgraph is likely to reflect major characteristics of the FIN.

The density of a directed graph is given by the ratio $\rho = M/[N(N-1)]$ between the number of directed edges (links) M of the graph and the total number of possible links, $N(N-1)$, where N is the number of nodes in the graph. The $G_{29\times29}$ graph has $M = 536$ (binary) directed links from the maximum possible of $N(N-1) = 812$, and therefore, it is strongly interconnected, with a graph density of $\rho = 0.66$ (66%). Because it is an edge-complete subgraph of FIN, the density of $G_{29\times29}$ is expected to be comparable to that of the FIN.

The in-degrees of the $G_{29\times91}$ graph (i.e. the number of source areas projecting to each of 29 target areas, Fig. 12) range from 26 to 87 with a mean of $\langle k\rangle_{\text{in}} = 55.4$; their distribution (right side of figure) is concentrated around the mean. The density of the FIN was estimated as follows. Because every directed edge is an in-link to some node, the total number of edges M_{FIN} equals the total number of in-links in the FIN. We lack data on the in-links to nodes that were not injected, but we can assume that they are characterized by the same average in-degree as the 29 injected nodes. Assuming $M_{\text{FIN}} \approx \langle k\rangle_{\text{in}} N_{\text{FIN}} = 5,071$ for the FIN ($G_{91\times91}$) leads to the prediction $\rho_{\text{FIN}} = M_{\text{FIN}}/[N_{\text{FIN}}(N_{\text{FIN}}-1)] \approx \langle k\rangle_{\text{in}}/(N_{\text{FIN}}-1) \approx 0.62$ (62%), which is of the same order as the density for the edge-complete graph $G_{29\times29}$.

A dominating set analysis on $G_{29\times91}$ provides further evidence that the FIN is indeed dense. In graph theory, a subset

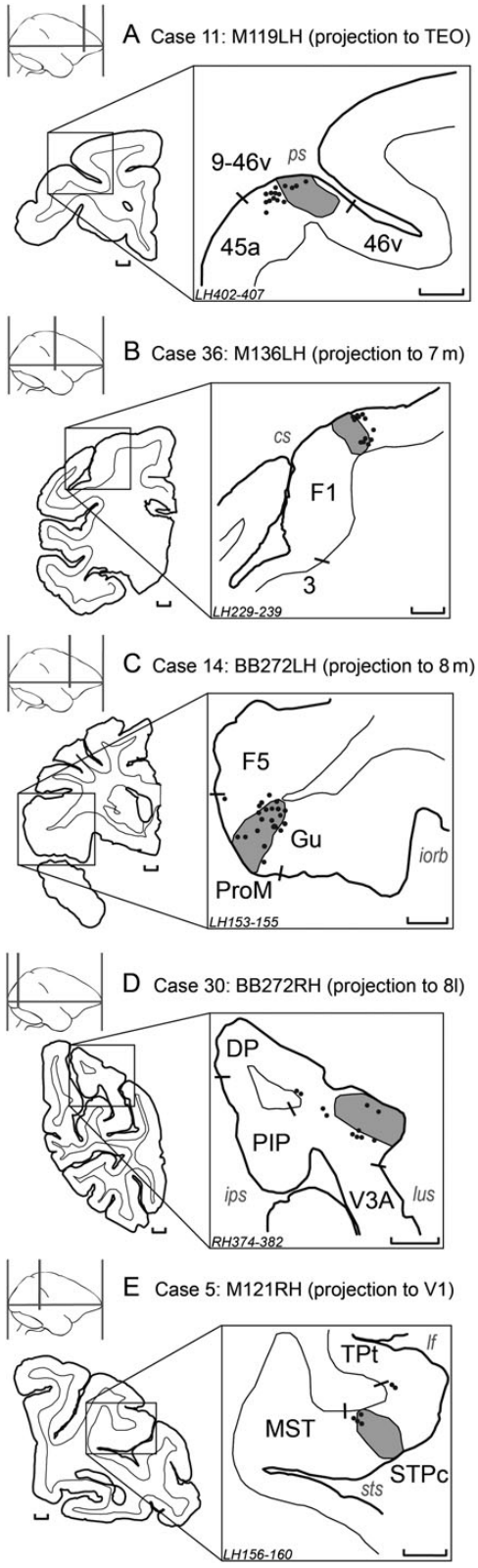

Figure 10. Positive identification of unidirectional pathways. Examples of contiguity of injection site and retrograde labeled neurons in unidirectional pathways. For a unidirectional projection $X \geq Y$, we show the labeled neurons in area X following injection in area Y. The injection site in area X is the injection site that failed to label neurons in area Y. Note that the injection site and the reported labeled neurons are in 2 different brains. Scale bars: 2 mm.

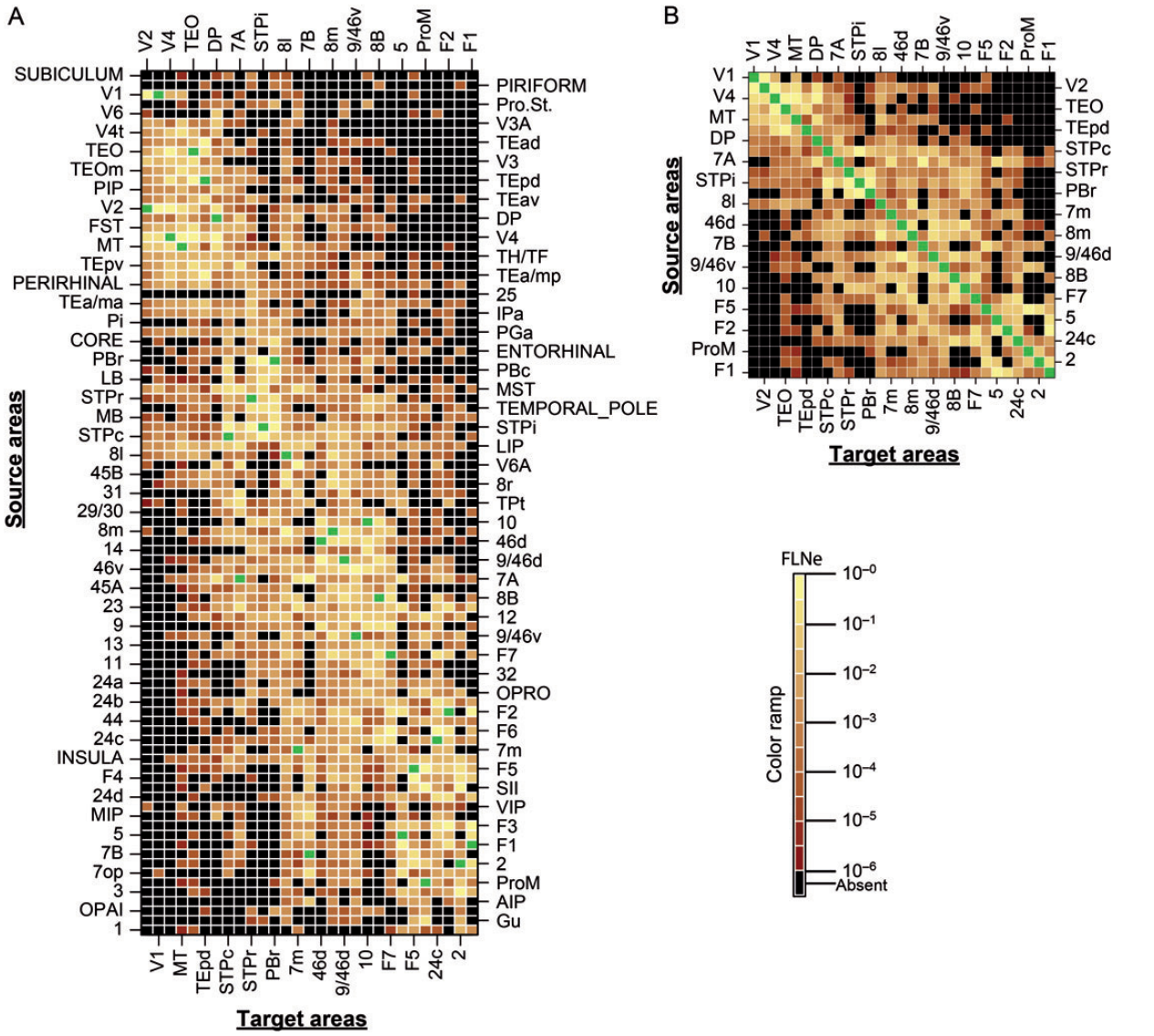

Figure 11. Weighted connectivity matrix. (*A*) Each row represents 1 of the 91 source areas; each column represents 1 of the 29 injected target areas. The color shows the strength of the projection as indicated by the color bar with black corresponding to absent connections and green for the intrinsic projections that are not included here. The row and column ordering was determined by a clustering algorithm based on similarity of the input and output profiles between areas (see the Materials and Methods section). (*B*) A weighted connectivity matrix for the 29 × 29 subgraph. For multiple injections, shading is based on geometric mean values.

D of nodes of a graph *G* with node set *V* is said to be dominating *G*, if all elements of *V* have a link to at least one node in *D* (Kulli and Sigarkanti 1991). Here, we modify this definition slightly by saying that *D* dominates *x*% of the nodes of *G*, if an *x*% of "all" nodes in *V* are linked to one or more nodes in *D*. The *x*% = 100% corresponds to "full" domination. This definition includes also nodes from *D*. The minimum dominating set (MDS) D_{min} is defined as the one that fully dominates *G* and it has the smallest size (number of nodes). For all sets of 2 target area combinations from the 29 target areas (406 pairs), 26.6% of them dominate 90–100% of the 91 areas (see Supplementary Table 5). One pair of areas (8l, 7m) receives projections from all 91 areas, revealing an MDS size of 2.

A low MDS indicates either a very dense graph or a scale-free graph (usually dominated by its hubs) (Barabasi and Albert 1999). The in-degree distribution (Fig. 12) is "inconsistent" with a scale free graph, as is the fact that slightly increasing the size of dominating sets to include 3, 4, and more nodes quickly increases their number. For area triples there are 69 dominating sets (1.88% of 3654), and for sets of 4 areas, there are 1,978 (8.33% of 23 751). Moreover, all combinations of 8 sites (out of 29, ~4.29 million) will dominate at least 90% of all the areas (see Supplementary Table 5). As more injections add links but not new nodes, they can only enhance these strong domination effects, confirming that the FIN is indeed a dense graph when considered in terms of binary connectivity.

Discussion

By characterizing the strength of 1,615 identified interareal projections, this study provides the most extensive quantitative analysis to date on cortico-cortical connectivity in the

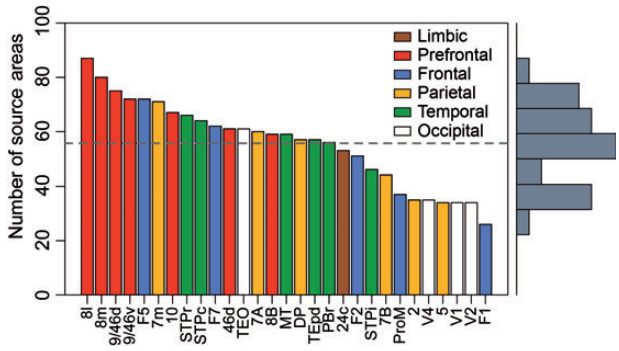

Figure 12. In-degree distribution. The number of areas projecting to each of the target areas of this study. Horizontal dashed line indicates the mean in-degree 57.4.

macaque. While nearly a thousand of these projections had been previously described, published data on interareal connection weights has been extremely limited. Most of the connection weights we report are based on only a single injection, but we provide evidence that these measurements are generally within an order of magnitude of the average connection weight for the subregion of the area that was injected. In addition, we report not only the presence but also the weights for 579 NFP. Altogether, this provides a reasonably accurate portrayal of the connectivity profiles for the 29 injected areas and provides $G_{29\times29}$ and $G_{29\times91}$ subgraphs constructed with consistent criteria. Our analysis also provides valuable inferences regarding statistical characteristics of the entire cortical connectivity graph. To place these findings into a broader context, several issues warrant discussion.

Technical Considerations and Limitations

We used retrograde tracers that show high sensitivity and restricted uptake zones, the latter making it possible to verify their restriction to a single cortical area (for a detailed discussion of the relative merits of the tracers used here, see Supplementary material in Markov et al. 2011). While most of the injection sites were entirely restricted to the cortical gray matter, in a few there was minor encroachment into immediately subjacent white matter (see the Materials and Methods section and Supplementary Fig. 6). In such cases, a small proportion of labeled neurons may have arisen from fibers of passage. However, this is unlikely to be a major confound, especially since the fibers immediately under the gray matter mainly arise from the nearby cortex, that is, predominantly the same cortical area (Schmahmann and Pandya 2009).

When combined with close section intervals and full hemisphere scanning, these tracers revealed many NFP for each area injected and enabled estimation of connection weight for each projection. However, there are also limitations to the methods used. For instance, there are many alternative parcellation schemes for the macaque cortex, some of which are finer-grained than the 91-area parcellation we used. Nevertheless, our M132 parcellation has been mapped to the macaque F99 atlas, which contains accurate surface maps for 15 other published parcellations (Van Essen, Glasser, Dierker, Harwell 2011), thereby enabling detailed cross-parcellation comparisons. In addition, we report all injection sites by their stereotaxic coordinates in the F99 atlas space. This provides an even finer granularity for objectively comparing our connectivity data to alternative parcellation schemes and to other data modalities such as functional connectivity revealed by functional magnetic resonance imaging (fMRI) (Vincent et al. 2007) and structural connectivity revealed by diffusion imaging and tractography (Rushworth et al. 2009). It would be of interest to determine a quantitative connectivity matrix using one or more alternative parcellations applied to each of the cortical injection cases. Unfortunately, technical considerations make this an enormous undertaking that was not feasible for the present study.

Sampling Strategies and Statistical Methodologies

Scannell et al. (2000) emphasized the importance of sampling and statistical methodologies in efforts to quantify cortical connectivity. Conventional approaches typically involve repeat injections into each cortical area and examination of connectivity using only a small fraction of the available histological sections, and averaging of connectivity data across multiple cases. We chose an alternative strategy that includes sampling histological sections at high density and across the entire hemisphere, thereby capturing as much data as are feasible and also reducing variability related to brain morphology (Falchier et al. 2002; Vezoli et al. 2004; Markov et al. 2011). We first analyzed the strengths and limitations of the single-injection approach by quantitatively analyzing repeat injections in 4 areas (14 injections total). We then proceeded to analyze connectivity profiles for single injections in each of 25 areas.

The repeat-injection analysis indicates that connectivity patterns across animals are remarkably consistent, except for very sparse projections. This was previously shown for central visual field injections in areas V1, V2, and V4 (Markov et al. 2011) and is extended in the present study to area 10, a higher order area with about twice as many inputs as the early visual areas (Fig. 11). Projections having more than 10 neurons on average occurred consistently in repeat injections, with just 2 exceptions, and therefore can be considered stable projections. For very sparse projections, the probability of at least one false-negative increases with the number of injections (Fig. 5*B*). False-negatives are also more likely for areas such as area 10 that are connected to a larger number of other areas (Fig. 3*A*). The median number of estimated extrinsic neurons per hemisphere labeled by one of our repeat injections is 187,000 (interquartile range: 98,000–280,000), which gives a lower limit to the reliability of the FLNe of $<6\times10^{-5}$.

All 4 repeat-injection areas showed a distribution of FLNe strengths well fit by a lognormal distribution whose variability is described by a negative binomial distribution. The dispersion parameter for each area lies within a limited range (θ between 5 and 9). The 95% confidence intervals computed for individual injections into areas V1, V2, V4, and 10 include 97% of the mean values for the repeat injections. These data empirically confirm the capacity of our statistical analysis to predict the observed variance. The lognormal distribution of ordered FLNe values for the 25 single injections is similar to those for the 4 repeat-injection areas. Hence, it is reasonable to use the negative binomial model derived from the repeat injections to estimate the 95% confidence intervals for the single injections as well. The lognormal distribution observed for all injections indicates that sparse connections are part of

an impressively broad and essentially continuous range of connection weights.

Many cortical areas show major internal heterogeneity in their connectivity patterns that exceeds the variability reported here for repeat injections that were localized to a particular areal subregion. This is well documented for the peripheral versus central representations of V1, V2, and V4 (Falchier et al. 2002) and the body representation of F2 (Johnson et al. 1996; Matelli et al. 1998; Tanne-Gariepy et al. 2002; Luppino et al. 2003). This cautionary note also applies to other topographically organized sensory-motor areas, and it might apply to higher-order areas as well (Burman et al. 2011). This underscores the importance of accurately specifying the location of the injection sites and the labeled neurons, in the context of a consistent database as provided in the present study (cf. Fig. 7 and see Supplementary Figs 2 and 4).

Variability

There are other sources of variability besides those just discussed (statistical fluctuations and regional heterogeneity within an area). All 4 of our repeat injections showed considerable variability, even for projections having moderate or strong FLNe values. Some of the variability may be attributable to imperfect delineation of areal boundaries for the various source areas. However, there is essentially no uncertainty in the boundaries of area V1; yet, the variability of V1 inputs to V4 exceeds that of many other source areas (see Fig. 11*C* in Markov et al. 2011). Moreover, we saw only a modest reduction in variability of the repeat injections in areas V1, V2, V4, and 10 (Fig. 3*C*) when the areas were grouped into regions (Fig. 3*D*).

For the above reasons, we consider it highly likely that there are genuine individual differences in connection strength that along with the lognormal distribution is a characteristic feature of interareal pathways. Whether such variability is related to experience during the development of the animal and/or individual differences in behavioral capacities is an important question that may become accessible to future noninvasive imaging studies (see below). We also note that the connection strengths reported here are (except in one case, see Supplementary Table 2) specifically for *M. fascicularis*; the values might vary for other macaque species, including the widely studied rhesus macaque (*M. mulatta*).

Newly found Projections

While the NFP are sparser than the known connections, overall their weight distribution overlaps with that of the known connections (Fig. 9). Further, repeat injections in areas V1, V2, V4, and 10 showed that 58% of NFP are present after each repeat injection and are therefore classified as consistent. We have compared the consistency of the NFP with that of the known projections in these repeat injections. This shows that at similar weights, the consistency of the NFP is equal to that of the known connections (see Supplementary Fig. 5).

Given the overlap of the FLNe values of known connections and NFP, why were the NFP detected here and not in previous reports? One factor is that we scrutinized the entire hemisphere for labeled cells at high magnification and at close section intervals (240 µm). Another is that most NFP are long-distance connections that may have been missed in studies that did not closely scrutinize distant cortical regions. A third is that some investigators may have assumed a priori that very sparse connections are functionally insignificant and could be safely ignored. Finally, as already noted, some connections we report as NFP might reflect cross-study differences in the designation of areal boundaries in individual cases.

The general finding is that cortical areas containing back labeled cells form a relatively continuous field comprising multiple areas as illustrated in Figure 7. On the whole, the NFP tend to complete the region of labeling formed by the known connections. A correlate of this is that in the 29 injections, 75% of NFP share borders with areas with known connections. Hence, in Figure 6 and Supplementary Figure 2, there are multiple examples of labeled neurons in NFP that could be included in a known connection by shifting a border, and in some instances, the shift would result in an unjustified increase in the dimensions of the known area. However, following random fusing of "all" possible pairs of adjacent areas shows that 25% NFP remain (data not shown). So while shifting borders could reduce the NFP, it would mean that we abandon a consistent atlas with an objective parcellation for one where area dimensions are dictated by labeling patterns. Besides decreasing the NFP, such a parcellation process would also tend to erase another aspect of the present findings, namely that there is a drop in the weight of connectivity towards the periphery of the region of labeled neurons and that neighboring areas share similar connectivity, even when labeling levels are very low.

Reciprocity

Previous reports provided scant evidence of unidirectional connectivity in the cortex (Felleman and Van Essen 1991). However, few experimental studies have directly tested unidirectionality because it is technically not easy. For example, using a bidirectional tracer such as WGA-HRP is not appropriate. This is because the high levels of recurrent connectivity in the source area (Braitenberg and Schüz 1998; Markov et al. 2011) can lead to labeled axon terminals in the vicinity of the retrogradely labeled cells that can be mistaken for long-distance anterograde labeling from the injected target area. Our evidence for unidirectionality is susceptible to error because the reciprocity of connections could only be tested using injections in different animals. However, this error cannot at present be overcome given that diffusion tensor imaging and tractography do not detect direction and existing tracing techniques, including BDA and labeled amino acids, show bidirectional transport (LeVay and Sherk 1983; da Costa and Martin 2011).

In the present study, reciprocity of cortical connectivity was unexpectedly low: There was evidence for unidirectionality for 33% of connections, and over 40% of bidirectional connections were strongly asymmetrical. However, areal heterogeneity may be a confounding factor for many of the apparent unidirectional connections reported in the present study. Positive confirmation via superposition of injection sites and retrograde labeling suggests that a minimum of 10% of all cortical pathways are genuinely unidirectional.

Matrix Density

The 29 injections reported here revealed many long-distance NFP having FLNe values that overlap with the known connections and showed similar consistency. This gave rise to a connectivity density (i.e. the number of existing connections expressed as a percentage of the maximum number of possible connections) of 66%. Further graph theoretic analysis allowed us to infer that the binary FIN is dense and that this is therefore a characteristic feature of the macaque cortex. High densities are necessarily accompanied by a short average path length across the cortex and will impact on large-scale models of cortical networks (Young 1993; Sporns et al. 2000; Honey et al. 2007).

Low cortical matrix densities have been reported in estimates based on large data sets compiled across studies (e.g. Young 1993, who reported a density of ~15%). The lower density in these large datasets might suggest that connections between specialized cortical systems are uncommon. However, subsequent studies have revealed numerous connections between functional systems, for example, between early auditory and visual areas (Falchier et al. 2002). In this respect, we found that NFP signficantly span greater distances and more frequently link areas in different regions than do the known connections (Markov et al. in preparation). If the analysis were restricted to previously known connections, the estimated density for the entire hemisphere would decrease to 45%, similar to that predicted for the visual system alone by Felleman and Van Essen (1991) and Jouve et al. 1998.

Conclusion

Increasing brain size has been suggested to result in decreased connectivity (Ringo 1991). A reduction in connectivity could be associated with lower weights of long-range pathways with respect to local connectivity or with a reduction in the number of pathways (at least in relation to the total number of area-to-area combinatorial possibilities). A decrease in weight values with increasing size is supported by the comparison of interareal connectivity in primate brains of different sizes (Palmer and Rosa 2006). Changes in the frequency of long-distance connections with changes in brain size would be associated with a change in density of the cortical matrix. In this respect, it is notable that the mouse cortex has a very high density of its interareal graph in comparison to the present findings in the larger macaque brain (Wang et al. 2012).

The human cerebral cortex is 9-fold greater in surface area than the macaque and probably contains a maximum of 150–200 cortical areas compared with the estimated maximum of 130–140 in the macaque (Van Essen, Glasser, Dierker, Harwell 2011; Van Essen, Glasser, Dierker, Harwell, Coalson 2011). What are the major differences in cortico-cortical connectivity in the 2 species? Although the human cortex is not amenable to anatomical tracer studies, the emergence of non-invasive neuroimaging methods, including tractography using diffusion imaging and functional connectivity using resting-state fMRI, opens the possibility of learning much about the human connectome (Behrens and Sporns 2012; Van Essen and Ugurbil 2012; Van Essen et al. 2012). Numerous noninvasive brain imaging studies carried out in primates using brain parcellations ranging from 45 to 90 areas report wide ranging densities, from 7% to over 50% (He et al. 2007; Chen et al. 2008; Hagmann et al. 2008; Iturria-Medina et al. 2008; Gong et al. 2009; Li et al. 2009). The wide range of densities might reflect either differences in thresholding or technical difficulties (Jones 2010; Jbabdi and Johansen-Berg 2011; Behrens and Sporns 2012; Van Essen and Ugurbil 2012).

While it is widely presumed that functional connectivity (i.e. functional correlated fMRI signals across the cortex) are constrained by the underlying structural connectivity, the nature of this relationship remains to be understood (Bressler and Menon 2010). For instance, while there is evidence for a good correlation between functional connectivity and strong short-distance connections, this is not the case for the more numerous long-distance connections (Honey et al. 2009; Adachi et al. 2012). A recent modeling study showed that including anatomical directionality and weight led to more realistic biologically modeled brain dynamics (Knock et al. 2009). One issue of particular interest is the relative importance of projections of different strengths. There are numerous examples of causative interaction between weakly connected areas where the direct cortico-cortical pathway may play a functional role (Ekstrom et al. 2008; Wang et al. 2008). The combination of weight "and" distance of connections may be important for understanding large-scale temporal dynamics (Honey et al. 2007). Sparse long-distance connections, conceivably via nonlinear phenomena such as "contraction dynamics", may have disproportionate effects relative to the far more dense intrinsic and intermediate-distance connections (Wang and Slotine 2005).

Supplementary Material

Supplementary material can be found at: http://www.cercor.oxfordjournals.org/.

Funding

This work was supported by FP6-2005 IST-1583 (H.K.), FP7-2007 ICT-216593 (H.K.), ANR-05-NEUR-088 (H.K.), ANR-11-BSV4-0051 (H.K.), Region Rhône-Alpes CIBLE 11-010869 (H.K.), LabEx CORTEX (H.K.), NIH R01-MH-60974 (D.C.V.E.), and in part by HDTRA-1-09-1-0039 and NSF BCS-0826958 (Z.T. and M.M.E.R.). Funding to pay the Open Access publication charges for this article was provided by ANR-11-BSV4-0051.

Notes

The authors thank D. Autran, A. Batardiere, J. Beneyton, A. Kennedy, and S. Zouaoui for histological assistance and B. Beneyton, F. Piolat, M. Seon, and M. Valdebenito for animal husbandry. E. Reid for cortical surface reconstruction and V. Vezoli for administrative assistance. D. Dierker, J. Harwell, and L.J. Pilaz for software development. *Conflict of Interest*: None declared.

References

Adachi Y, Osada T, Sporns O, Watanabe T, Matsui T, Miyamoto K, Miyashita Y. 2012. Functional connectivity between anatomically unconnected areas is shaped by collective network-level effects in the macaque cortex. Cereb Cortex. 22:1586–1592.

Aflalo TN, Graziano MS. 2011. Organization of the macaque extrastriate visual cortex re-examined using the principle of spatial continuity of function. J Neurophysiol. 105:305–320.

Barabasi AL, Albert R. 1999. Emergence of scaling in random networks. Science. 286:509–512.

Barbas H, Hilgetag CC, Saha S, Dermon CR, Suski JL. 2005. Parallel organization of contralateral and ipsilateral prefrontal cortical projections in the rhesus monkey. BMC Neurosci. 6:32.
Barbas H, Pandya DN. 1987. Architecture and frontal cortical connections of the premotor cortex (area 6) in the rhesus monkey. J Comp Neurol. 256:211–228.
Barbas H, Pandya DN. 1989. Architecture and intrinsic connections of the prefrontal cortex in the rhesus monkey. J Comp Neurol. 286:353–375.
Barbas H, Rempel-Clower N. 1997. Cortical structure predicts the pattern of corticocortical connections. Cereb Cortex. 7:635–646.
Barone P, Batardiere A, Knoblauch K, Kennedy H. 2000. Laminar distribution of neurons in extrastriate areas projecting to visual areas V1 and V4 correlates with the hierarchical rank and indicates the operation of a distance rule. J Neurosci. 20:3263–3281.
Batardiere A, Barone P, Dehay C, Kennedy H. 1998. Area-specific laminar distribution of cortical feedback neurons projecting to cat area 17: Quantitative analysis in the adult and during ontogeny. J Comp Neurol. 396:493–510.
Behrens TE, Sporns O. 2012. Human connectomics. Curr Opin Neurobiol. 22:144–153.
Boccaletti S, Latora V, Moreno Y, Chavez M, Hwang DU. 2006. Complex networks: Structure and dynamics. Phys Rep. 424:175–308.
Bohland JW, Wu C, Barbas H, Bokil H, Bota M, Breiter HC, Cline HT, Doyle JC, Freed PJ, Greenspan RJ *et al*. 2009. A proposal for a coordinated effort for the determination of brainwide neuroanatomical connectivity in model organisms at a mesoscopic scale. PLoS Comput Biol. 5:e1000334.
Boussaoud D, Desimone R, Ungerleider LG. 1991. Visual topography of area TEO in the macaque. J Comp Neurol. 306:554–575.
Boussaoud D, Ungerleider LG, Desimone R. 1990. Pathways for motion analysis: Cortical connections of the medial superior temporal and fundus of the superior temporal visual areas in the macaque. J Comp Neurol. 296:462–495.
Braitenberg V, Schüz A. 1998. Cortex: statistics and geometry of neuronal connectivity. Berlin, Heidelberg, New York: Springer-Verlag.
Bressler SL, Menon V. 2010. Large-scale brain networks in cognition: Emerging methods and principles. Trends Cogn Sci. 14:277–290.
Bretz F, Hothorn T, Westfall P. 2010. Multiple comparisons using R. Boca Raton: CRC Press.
Bullmore E, Sporns O. 2009. Complex brain networks: Graph theoretical analysis of structural and functional systems. Nat Rev Neurosci. 10:186–198.
Burman KJ, Reser DH, Yu HH, Rosa MG. 2011. Cortical Input to the frontal pole of the marmoset monkey. Cereb Cortex. 21:1712–1737.
Caminiti R, Genovesio A, Marconi B, Mayer AB, Onorati P, Ferraina S, Mitsuda T, Giannetti S, Squatrito S, Maioli MG *et al*.. 1999. Early coding of reaching: Frontal and parietal association connections of parieto-occipital cortex. Eur J Neurosci. 11:3339–3345.
Chen ZJ, He Y, Rosa-Neto P, Germann J, Evans AC. 2008. Revealing modular architecture of human brain structural networks by using cortical thickness from MRI. Cereb Cortex. 18:2374–2381.
Cipolloni PB, Pandya DN. 1999. Cortical connections of the frontoparietal opercular areas in the rhesus monkey. J Comp Neurol. 403:431–458.
Clavagnier S, Falchier A, Kennedy H. 2004. Long-distance feedback projections to area V1: Implications for multimodal integration, spatial awarness and visual consciousness. Cogn Affect Behav Neurosci. 4:117–126.
da Costa NM, Martin KA. 2011. How thalamus connects to spiny stellate cells in the cat's visual cortex. J Neurosci. 31:2925–2937.
Dum RP, Strick PL. 1991. The origin of corticospinal projections from the premotor areas in the frontal lobe. J Neurosci. 11:667–689.
Ekstrom LB, Roelfsema PR, Arsenault JT, Bonmassar G, Vanduffel W. 2008. Bottom-up dependent gating of frontal signals in early visual cortex. Science. 321:414–417.
Falchier A, Clavagnier S, Barone P, Kennedy H. 2002. Anatomical evidence of multimodal integration in primate striate cortex. J Neurosci. 22:5749–5759.
Felleman DJ, Burkhalter A, Van Essen DC. 1997. Cortical connections of areas V3 and VP of macaque monkey extrastriate visual cortex. J Comp Neurol. 379:21–47.
Felleman DJ, Van Essen DC. 1991. Distributed hierarchical processing in the primate cerebral cortex. Cereb Cortex. 1:1–47.
Friston K. 2010. The free-energy principle: A unified brain theory? Nat Rev Neurosci. 11:127–138.
Gattass R, Nascimento-Silva S, Soares JG, Lima B, Jansen AK, Diogo AC, Farias MF, Botelho MM, Mariani OS, Azzi J *et al*.. 2005. Cortical visual areas in monkeys: Location, topography, connections, columns, plasticity and cortical dynamics. Philos Trans R Soc Lond B Biol Sci. 360:709–731.
Ghosh S, Gattera R. 1995. A comparison of the ipsilateral cortical projections to the dorsal and ventral subdivisions of the macaque premotor cortex. Somatosens Mot Res. 12:359–378.
Godschalk M, Mitz AR, van Duin B, van der Burg H. 1995. Somatotopy of monkey premotor cortex examined with microstimulation. Neurosci Res. 23:269–279.
Gong G, He Y, Concha L, Lebel C, Gross DW, Evans AC, Beaulieu C. 2009. Mapping anatomical connectivity patterns of human cerebral cortex using in vivo diffusion tensor imaging tractography. Cereb Cortex. 19:524–536.
Goodhill GJ, Simmen MW, Willshaw DJ. 1995. An evaluation of the use of multidimensional scaling for understanding brain connectivity. Philos Trans R Soc Lond B Biol Sci. 348:265–280.
Graziano MS, Aflalo TN. 2007. Rethinking cortical organization: Moving away from discrete areas arranged in hierarchies. Neuroscientist. 13:138–147.
Hagmann P, Cammoun L, Gigandet X, Meuli R, Honey CJ, Wedeen VJ, Sporns O. 2008. Mapping the structural core of human cerebral cortex. PLoS Biol. 6:e159.
He SQ, Dum RP, Strick PL. 1993. Topographic organization of corticospinal projections from the frontal lobe: Motor areas on the lateral surface of the hemisphere. J Neurosci. 13:952–980.
He Y, Chen ZJ, Evans AC. 2007. Small-world anatomical networks in the human brain revealed by cortical thickness from MRI. Cereb Cortex. 17:2407–2419.
Honey CJ, Kotter R, Breakspear M, Sporns O. 2007. Network structure of cerebral cortex shapes functional connectivity on multiple time scales. Proc Natl Acad Sci USA. 104:10240–10245.
Honey CJ, Sporns O, Cammoun L, Gigandet X, Thiran JP, Meuli R, Hagmann P. 2009. Predicting human resting-state functional connectivity from structural connectivity. Proc Natl Acad Sci USA. 106:2035–2040.
Iturria-Medina Y, Sotero RC, Canales-Rodriguez EJ, Aleman-Gomez Y, Melie-Garcia L. 2008. Studying the human brain anatomical network via diffusion-weighted MRI and Graph Theory. Neuroimage. 40:1064–1076.
Janson S, Luczak T, Rucinski A. 2000. Random graphs. New York: Wiley-Interscience.
Jbabdi S, Johansen-Berg H. 2011. Tractography—where do we go from here? Brain Connectivity. 1:169–183.
Johnson PB, Ferraina S. 1996. Cortical networks for visual reaching: Intrinsic frontal lobe connectivity. Eur J Neurosci. 8:1358–1362.
Johnson PB, Ferraina S, Bianchi L, Caminiti R. 1996. Cortical networks for visual reaching: Physiological and anatomical organization of frontal and parietal lobe arm regions. Cereb Cortex. 6:102–119.
Jones DK. 2010. Challenges and limitations of quantifying brain connectivity in vivo with diffusion MRI. Imaging Med. 2:341–355.
Jones EG, Coulter JD, Hendry SH. 1978. Intracortical connectivity of architectonic fields in the somatic sensory, motor and parietal cortex of monkeys. J Comp Neurol. 181:291–347.
Jouve B, Rosenstiehl P, Imbert M. 1998. A mathematical approach to the connectivity between the cortical visual areas of the macaque monkey. Cereb Cortex. 8:28–39.
Kaas JH, Collins CE. 2001. The organization of sensory cortex. Curr Opin Neurobiol. 11:498–504.
Kennedy H, Bullier J. 1985. A double-labeling investigation of the afferent connectivity to cortical areas V1 and V2 of the macaque monkey. J Neurosci. 5:2815–2830.

Knock SA, McIntosh AR, Sporns O, Kotter R, Hagmann P, Jirsa VK. 2009. The effects of physiologically plausible connectivity structure on local and global dynamics in large scale brain models. J Neurosci Methods. 183:86–94.
Koch C. 2004. The quest for consciousness: a neurobiological approach. Englewood, CO: Roberts and Company.
Kotter R. 2004. Online retrieval, processing, and visualization of primate connectivity data from the CoCoMac database. Neuroinformatics. 2:127–144.
Kulli VR, Sigarkanti SC. 1991. Inverse domination in graphs. Nat Acad Sci Lett. 14:473–475.
LeVay S, Sherk H. 1983. Retrograde transport of [3H]proline: A widespread phenomenon in the central nervous system. Brain Res. 271:131–134.
Lewis JW, Van Essen DC. 2000. Corticocortical connections of visual, sensorimotor, and multimodal processing areas in the parietal lobe of the macaque monkey. J Comp Neurol. 428:112–137.
Li Y, Liu Y, Li J, Qin W, Li K, Yu C, Jiang T. 2009. Brain anatomical network and intelligence. PLoS Comput Biol. 5:e1000395.
Luppino G, Calzavara R, Rozzi S, Matelli M. 2001. Projections from the superior temporal sulcus to the agranular frontal cortex in the macaque. Eur J Neurosci. 14:1035–1040.
Luppino G, Rozzi S, Calzavara R, Matelli M. 2003. Prefrontal and agranular cingulate projections to the dorsal premotor areas F2 and F7 in the macaque monkey. Eur J Neurosci. 17:559–578.
Marconi B, Genovesio A, Battaglia-Mayer A, Ferraina S, Squatrito S, Molinari M, Lacquaniti F, Caminiti R. 2001. Eye-hand coordination during reaching. I. Anatomical relationships between parietal and frontal cortex. Cereb Cortex. 11:513–527.
Markov NT, Misery P, Falchier A, Lamy C, Vezoli J, Quilodran R, Gariel MA, Giroud P, Ercsey-Ravasz M, Pilaz LJ *et al*.. 2011. Weight consistency specifies regularities of macaque cortical networks. Cereb Cortex. 21:1254–1272.
Matelli M, Govoni P, Galletti C, Kutz DF, Luppino G. 1998. Superior area 6 afferents from the superior parietal lobule in the macaque monkey. J Comp Neurol. 402:327–352.
Morecraft RJ, Stilwell-Morecraft KS, Cipolloni PB, Ge J, McNeal DW, Pandya DN. 2012. Cytoarchitecture and cortical connections of the anterior cingulate and adjacent somatomotor fields in the rhesus monkey. Brain Res Bull. 87:457–497.
Mountcastle VB. 1997. The columnar organization of the neocortex. Brain. 120:701–722.
Newman MEJ. 2010. Networks: an introduction. New York: Oxford University Press.
Newman MEJ. 2003. The structure and function of complex networks. SIAM Rev. 45:167–256.
Palmer SM, Rosa MG. 2006. Quantitative analysis of the corticocortical projections to the middle temporal area in the marmoset monkey: Evolutionary and functional implications. Cereb Cortex. 16:1361–1375.
Paxinos G, Huang XF, Toga AW. 2000. The rhesus monkey brain in stereotaxic coordinates. San Diego, CA: Academic Press.
Perkel DJ, Bullier J, Kennedy H. 1986. Topography of the afferent connectivity of area 17 in the macaque monkey: A double-labelling study. J Comp Neurol. 253:374–402.
Petrides M, Pandya DN. 2009. Distinct parietal and temporal pathways to the homologues of Broca's area in the monkey. PLoS Biol. 7: e1000170.
Petrides M, Pandya DN. 1999. Dorsolateral prefrontal cortex: Comparative cytoarchitectonic analysis in the human and the macaque brain and corticocortical connection patterns. Eur J Neurosci. 11:1011–1036.
Petrides M, Pandya DN. 2006. Efferent association pathways originating in the caudal prefrontal cortex in the macaque monkey. J Comp Neurol. 498:227–251.
Petrides M, Pandya DN. 1984. Projections to the frontal cortex from the posterior parietal region in the rhesus monkey. J Comp Neurol. 228:105–116.
Rakic P. 1988. Specification of cerebral cortical areas. Science. 241:170–176.
Ringo JL. 1991. Neuronal interconnection as a function of brain size. Brain Behav Evol. 38:1–6.
Rockland KS. 1997. Element of cortical architecture: hierarchy revisited. In: Rockland KS, Kaas JH, Peters A, editors. Extrastriate cortex in primates. New York: Plenum press. p. 243–293.
Rockland KS, Saleem KS, Tanaka K. 1994. Divergent feedback connections from areasV4 and TEO in the macaque. Vis Neurosci. 11:579–600.
Rockland KS, Van Hoesen GW. 1994. Direct temporal-occipital feedback connections to striate cortex (V1) in the macaque monkey. Cereb Cortex. 4:300–313.
Rosa MG, Tweedale R. 2005. Brain maps, great and small: Lessons from comparative studies of primate visual cortical organization. Philos Trans R Soc Lond B Biol Sci. 360:665–691.
Rubinov M, Sporns O. 2010. Complex network measures of brain connectivity: Uses and interpretations. Neuroimage. 52:1059–1069.
Rushworth MFS, Boorman E, Mars RB. 2009. Comparing brain connections in different species using diffusion weighted imaging In: Johansen-Berg H, Behrens TEJ, editors. Diffusion MRI: from quantitative measurement to in vivo neuroanatomy. Amsterdam: Academic Press. pp. 445–460.
Saleem KS, Logothetis NK. 2007. A combined MRI and histology atlas of the rhesus monkey brain in stereotaxic coordinates. Amsterdam, Boston: Elsevier/Academic Press.
Scannell JW, Grant S, Payne BR, Baddeley R. 2000. On variability in the density of corticocortical and thalamocortical connections. Philos Trans R Soc Lond B Biol Sci. 355:21–35.
Schmahmann JD, Pandya DN. 2009. Fiber pathways of the brain. New York: Oxford University Press.
Schüz A, Miller M. 2002. Cortical areas: unity and diversity. London: Taylor and Francis.
Seltzer B, Pandya DN. 1989. Frontal lobe connections of the superior temporal sulcus in the rhesus monkey. J Comp Neurol. 281:97–113.
Sporns O, Honey CJ, Kotter R. 2007. Identification and classification of hubs in brain networks. PLoS One. 2:e1049.
Sporns O, Tononi G, Edelman GM. 2000. Theoretical neuroanatomy: Relating anatomical and functional connectivity in graphs and cortical connection matrices. Cereb Cortex. 10:127–141.
Sporns O, Zwi JD. 2004. The small world of the cerebral cortex. Neuroinformatics. 2:145–162.
Stephan KE, Kamper L, Bozkurt A, Burns GA, Young MP, Kotter R. 2001. Advanced database methodology for the Collation of Connectivity data on the Macaque brain (CoCoMac). Philos Trans R Soc Lond B Biol Sci. 356:1159–1186.
Stepniewska I, Kaas JH. 1996. Topographic patterns of V2 cortical connections in macaque monkeys. J Comp Neurol. 371:129–152.
Takada M, Nambu A, Hatanaka N, Tachibana Y, Miyachi S, Taira M, Inase M. 2004. Organization of prefrontal outflow toward frontal motor-related areas in macaque monkeys. Eur J Neurosci. 19:3328–3342.
Tanne-Gariepy J, Rouiller EM, Boussaoud D. 2002. Parietal inputs to dorsal versus ventral premotor areas in the macaque monkey: Evidence for largely segregated visuomotor pathways. Exp Brain Res. 145:91–103.
Van Essen DC. 2004. Surface-based approaches to spatial localization and registration in primate cerebral cortex. Neuroimage. 23(Suppl 1):S97–S107.
Van Essen DC, Glasser MF, Dierker D, Harwell J. 2012. Cortical parcellations of the macaque monkey analyzed on surface-based atlases. Cereb Cortex. 22:2227–2240.
Van Essen DC, Glasser MF, Dierker D, Harwell J, Coalson T. 2012. Parcellations and hemispheric asymmetries of human cerebral cortex analyzed on surface-based atalses. Cereb Cortex. 22:2241–2262.
Van Essen DC, Harwell J, Hanlon D, Dickson J. 2005. Surface-based atlases and a database of cortical structure and function. In: Koslow SH, Subramaniam S, editors. Databasing the brain: from data to knowledge (neuroinformatics). NJ: John Wiley & Sons. p. 369–387.

Van Essen DC, Newsome WT, Maunsell JH, Bixby JL. 1986. The projections from striate cortex (V1) to areas V2 and V3 in the macaque monkey: Asymmetries, areal boundaries, and patchy connections. J Comp Neurol. 244:451–480.

Van Essen DC, Ugurbil K. 2012. The future of the human connectome. NeuroImage. 62:1299–1310.

Van Essen DC, Ugurbil K, Auerbach E, Barch D, Behrens TE, Bucholz R, Chang A, Chen L, Corbetta M, Curtiss SW *et al*. 2012. The Human Connectome Project: A data acquisition perspective. NeuroImage. http://www.ncbi.nlm.nih.gov/pubmed/22366334 [Epub ahead of print].

Vezoli J, Falchier A, Jouve B, Knoblauch K, Young M, Kennedy H. 2004. Quantitative analysis of connectivity in the visual cortex: Extracting function from structure. Neuroscientist. 10: 476–482.

Vincent JL, Patel GH, Fox MD, Snyder AZ, Baker JT, Van Essen DC, Zempel JM, Snyder LH, Corbetta M, Raichle ME. 2007. Intrinsic functional architecture in the anaesthetized monkey brain. Nature. 447:83–86.

Wang Q, Sporns O, Burkhalter A. 2012. Network analysis of corticocortical connections reveals ventral and dorsal processing streams in mouse visual cortex. J Neurosci. 32:4386–4399.

Wang W, Slotine JJ. 2005. On partial contraction analysis for coupled nonlinear oscillators. Biol Cybern. 92:38–53.

Wang Y, Celebrini S, Trotter Y, Barone P. 2008. Visuo-auditory interactions in the primary visual cortex of the behaving monkey: Electrophysiological evidence. BMC Neurosci. 9:79.

Watts DJ. 1999. Networks, Dynamics, and the small-world phenomenon. Am J Sociology. 105:493–527.

Watts DJ, Strogatz SH. 1998. Collective dynamics of small-world networks. Nature. 393:440–442.

Young MP. 1992. Objective analysis of the topological organization of the primate cortical visual system. Nature. 358:152–155.

Young MP. 1993. The organization of neural systems in the primate cerebral cortex. Proc R Soc Lond B Biol Sci. 252:13–18.

Zeki S. 1980. A direct projection from area V1 to area V3A of rhesus monkey visual cortex. Proc R Soc Lond B Biol Sci. 207:499–506.

Zeki S. 2005. Introduction: Cerebral cartography 1905–2005. Philos Trans R Soc Lond B Biol Sci. 360:651–652.

Zeki S, Shipp S. 1988. The functional logic of cortical connections. Nature. 335:311–317.

Zeki SM. 1978. The cortical projections of foveal striate cortex in the rhesus monkey. J Physiol. 277:227–244.